This dissertation has been
microfilmed exactly as received

66–14,210

EVANS, Winfield W., 1923–

EXPERIMENTAL EVALUATION OF MEDICAL SCANNERS.

The University of Oklahoma, Ph.D., 1966
Engineering, general

University Microfilms, Inc., Ann Arbor, Michigan

Downloaded from SHAREOK. Persistent Handle URL: https://hdl.handle.net/11244/2076

© Copyright by
WINFIELD W. EVANS
1967

THE UNIVERSITY OF OKLAHOMA

GRADUATE COLLEGE

EXPERIMENTAL EVALUATION OF MEDICAL SCANNERS

A DISSERTATION

SUBMITTED TO THE GRADUATE FACULTY

in partial fulfillment of the requirements for the

degree of

DOCTOR OF PHILOSOPHY

BY

WINFIELD W. EVANS

Oklahoma City, Oklahoma

1966

EXPERIMENTAL EVALUATION OF MEDICAL SCANNERS

APPROVED BY

DISSERTATION COMMITTEE

ACKNOWLEDGEMENTS

The author wishes to express his sincere appreciation to the following clinicians and their staff for their kind assistance and cooperation, without which this study could not have been carried out.

C. G. Coin, M.D., Chairman,
Department of Radiology
St. Anthony's Hospital
Oklahoma City, Oklahoma

R. B. Price, M.D., Chairman,
Department of Radiology
Baptist Memorial Hospital
Oklahoma City, Oklahoma

W. H. Reiff, M.D.,
3015 N. W. 59th
Oklahoma City, Oklahoma

W. H. Whitcomb, M.D., Director,
Radioisotope Service
V. A. Hospital
Oklahoma City, Oklahoma

TABLE OF CONTENTS

	Page
LIST OF TABLES	v
LIST OF ILLUSTRATIONS	vi
Chapter	
I. INTRODUCTION	1
II. BASIC THEORETICAL PRINCIPLES	3
III. EXPERIMENTAL PROCEDURES	26
IV. ANALYSIS OF RESULTS	30
V. CONCLUSION	38
BIBLIOGRAPHY	40
APPENDIX	41

LIST OF TABLES

Table		Page
1.	Comparison of Collimator Parameters	31
2.	Comparison of Scanner Sensitivities	32

LIST OF ILLUSTRATIONS

Figure		Page
1.	Collimator Geometry for One Channel	4
2.	Effect of Crystal Diameter on Solid Angle	6
3.	Intersection of Exit Pupil and Entrance Pupil Shadow	8
4.	Geometry for Vertical Displacement of Source	11
5.	The Linear Approximation	13
6.	The Quadratic Approximation	18
7.	Spectral Distribution of Hg-197--Ohio Nuclear	34
8.	Spectral Distribution of Hg-203--Ohio Nuclear	35
9.	Distribution for Hg-203--Picker 3"	42
10.	Distribution for Hg-197--Pho Dot 3"	43
11.	Distribution for I-131--Picker 5"	44
12.	Distribution for Co-57--Ohio Nuclear 8"	45
13.	Distribution for Co-57--Pho Dot 3"	46
14.	Distribution for Hg-197--Picker 5"	47
15.	Distribution for Co-57--Picker 3"	48
16.	Distribution for Hg-203--Picker 5"	49
17.	Large and Small Volume Scattering--Hg-203	50
18.	Large and Small Volume Scattering--Hg-197	51
19.	Large and Small Volume Scattering--I-131	52

EXPERIMENTAL EVALUATION OF MEDICAL SCANNERS

CHAPTER I

INTRODUCTION

Since the advent of nuclear reactors, the medical profession has made rapid and significant uses of various radioactive isotopes to expand and improve the diagnosis and treatment of many human diseases. One of the most intriguing of these applications is the field of Medical Radioisotope Scanning. In principle, scanning permits a clinician to determine the functional status of an organ, or system of organs, by detecting with external counters the presence or absence of radioactivity contained by or within an organ. This field has expanded rapidly during the past 10 years and has by no means achieved anthing resembling an equilibrium or saturation. On the contrary, the field is expanding so fast that new developments in scanning equipment and radiochemical compounds are reported almost on a monthly basis.

Due to the rapid acceptance of Medical Radioisotope Scanning by the medical profession, several commercial scanners are presently available. Each of these scanners has certain features that are due to compromises inherent in the design and applications of the particular device. It is almost a physical impossibility to design one scanner which does all things in an optimum fashion and which has the acceptance of all clinicians. Like other industries this forms the basis and

justification for healthy and beneficial competition.

This report is the result of an experimental evaluation performed in the field on a particular class of scanners (rectilinear) which comprise, at present, the majority of medical installations.

The scanners included in the evaluation are the Ohio-Nuclear 8" located at St. Anthony's Hospital, the Picker 5" located at Baptist Memorial Hospital, the Picker 3" located at the office of Dr. William Reiff, and the Nuclear-Chicago 3" Pho Dot located at V. A. Hospital. All of the installations are in Oklahoma City, Oklahoma.

This evaluation is an attempt to define the similarities and the differences that are the result of design compromises, and in certain instances, differences in operational techniques.

Although certain conclusions may be drawn from the results, the report is not intended to be used as a guide for the selection of a "best" scanner. The continued demand by the medical profession for highly specialized diagnostic techniques probably preclude the existence of a single "best instrument.

CHAPTER II

BASIC THEORETICAL PRINCIPLES

All rectilinear scanners have certain features which are similar. Basically, a scanning head containing the crystal, photomultiplier, collimator and preamplifier is mechanically driven in a 2 dimensional plane over an organ which contains radioactivity. The pulses from the detected gamma ray photons are amplified, electronically separated by a pulse height analyzer, and applied to a read-out device which is either mechanically or electrically coupled to the scanning head. The time-space concentration of pulses recorded by the read-out system represents, in principal, the radioactivity within the organ being scanned. Thus, rectilinear scanning is a 2 dimensional representation of a 3 dimensional distribution of radioactivity.

Since the gamma ray photons from a radioactive source are assumed to be isotropically distributed, the first and probably most important part of the scanner is the collimator. Harris[1] has summarized the necessity for multiple channel or focusing collimators. These collimators allow a greater number of photons to be detected per unit time while at the same time preserving the spatial distinction, or resolution, associated with the distribution of radioactivity.

To illustrate a few basic considerations and to emphasize the fact that compromises are essential, a brief derivation of certain geometrical

relationships is given. Figure 1 illustrates the basic description of a focusing collimator with 1 channel or 1 hole.

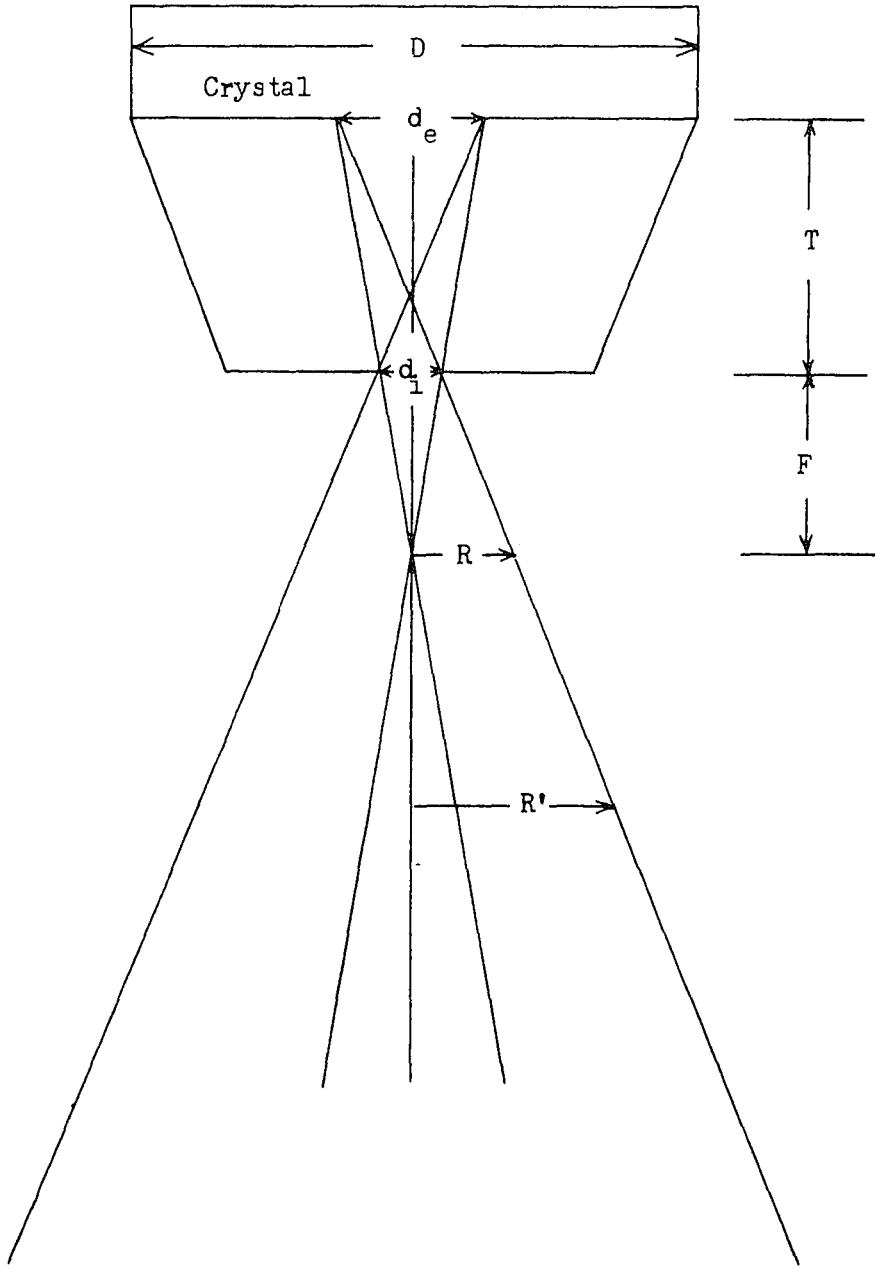

Figure 1: Collimator Geometry for One Channel

The geometrical relations are easily derived by similar triangles and by using a factor f which represents the fraction of the crystal which is exposed to the radioactivity located near the focal point F from the collimator surface. The extension to n holes or n channels is obvious and will be described later.

The essential features are the sensitivity to a point source, the sensitivity to a volume source whose dimensions are larger than twice the resolution distance R, and the resolution distance R.

Thus, the manufacturer has immediately at least 4 variables to choose: D--diameter of crystal, F--focal distance, T--collimator thickness, d_e--diameter of collimator hole at crystal (exit Pupil). The relationship between N_o (number of channels), d_e, f, and D eliminate n as a variable if d_e, f, and D are chosen.

Effect of Crystal Diameter on Solid Angle

Since most of the collimators have the same hole diameter at the crystal edge as at the crystal center, the effective solid angle is reduced from $N_o \Omega_o$ to a smaller value which depends on the crystal size and the distance F + T.

Figure 2 illustrates this geometry where it is assumed that the holes are distributed uniformly (approximately) over the collimator surface.

$$\text{Since } n_x = \frac{2\pi N_o \, x \, dx}{\pi X_o^2}$$

$$\text{and } \Omega_x = \frac{\frac{\pi}{4} d_e^2}{(F+T)^2 + x^2} \qquad \Omega_o = \frac{\frac{\pi}{4} d_e^2}{(F+T)^2}$$

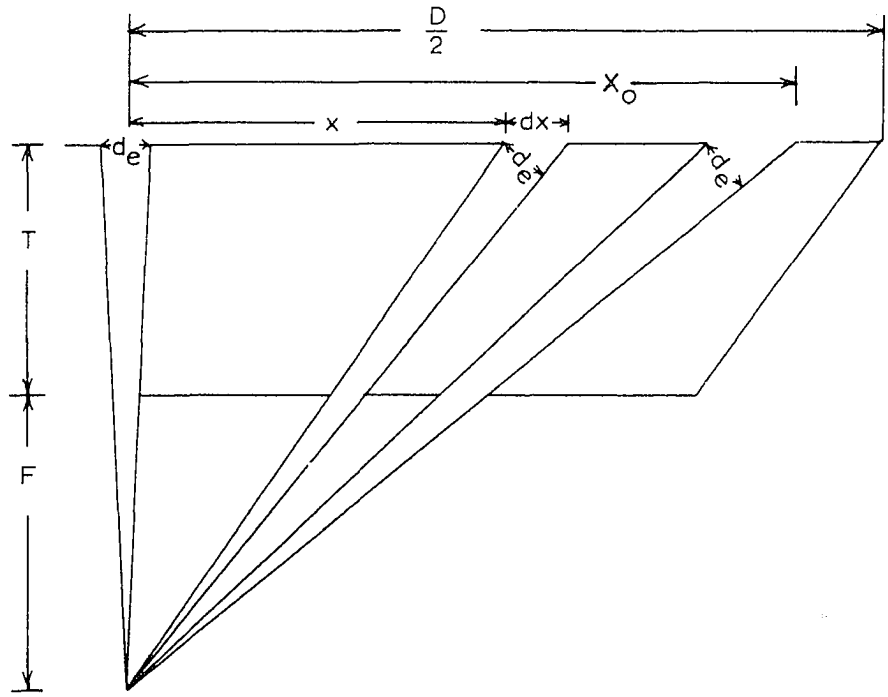

Figure 2: Effect of Crystal Diameter on Solid Angle

where N_o = total number of holes

X_o = collimator radius (center to outer hole)

n_x = number of holes between x and x + dx

$$\text{solid angle} = \int_0^{X_o} n_x \, (\text{solid angle})_x \, dx$$

$$(\text{solid angle})_{\text{total}} = \frac{\pi}{2} \frac{d_e^{\,2} N_o}{X_o^{\,2}} \int_0^{X_o} \frac{x \, dx}{(F + T)^2 + x^2}$$

$$\text{solid angle} = \frac{\pi}{4} \frac{d_e^{\,2} N_o}{X_o^{\,2}} \log \left(1 + \frac{X_o^{\,2}}{(F + T)^2}\right)$$

$$\Omega_{\text{total}} = \frac{\pi}{4} \frac{d_e^2 N_o}{X_o^2} \frac{X_o^2}{(F+T)^2} \left(1 - \frac{\frac{1}{2} X_o^2}{(F+T)^2} + \text{------}\right)$$

or

$$\Omega_{\text{total}} = \frac{\pi}{4} N_o \frac{d_e^2}{(F+T)^2} \left(1 - 1/2 \frac{X_o^2}{(F+T)^2} + \text{------}\right) \qquad (1)$$

$$\Omega_{\text{total}} = \frac{\pi}{4} \frac{d_e^2}{(F+T)^2} N_{eff}$$

where N_{eff} = Effective number of holes.

Thus, one cannot compare overall efficiencies of various collimators without taking into account the decrease in efficiency of the outer holes. For small crystals, of course, the second term in equation (1) is negligible and the total solid angle is N_o times the solid angle of a single channel.

Response to Lateral Displacement of a Point Source

To a first approximation the lateral response to a point source located at the focal plane may be derived by considering that the area at the exit pupil (d_e), which is subtended by a point at the focal plane, can be computed from the intersection of 2 circles. The first of these circles is the exit pupil proper, and the second circle is the one formed by the shadow of the entrance pupil (d_i) as the point moves laterally away from the focal point. For large T/d_e the resulting elliptical surfaces may be approximated by two intersecting circles of diameter d_e. Figure 3 illustrates the geometry of their approximation. The shaded area (a_x) divided by the circle area (A) gives the approximate response to the lateral displacement of a point source.

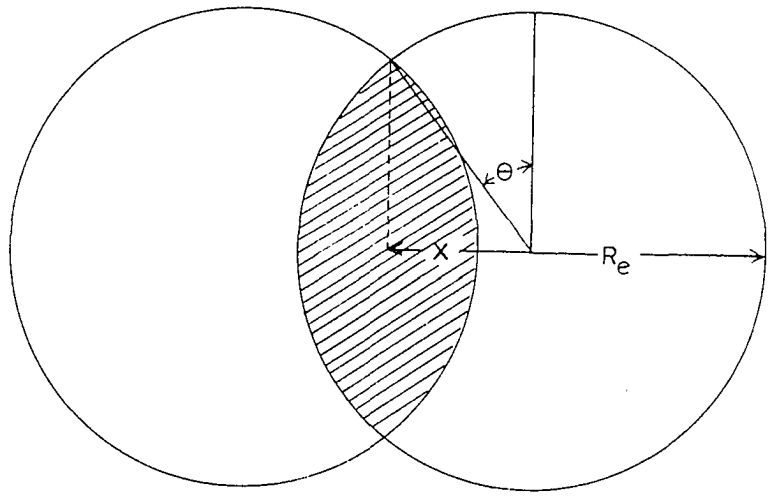

Figure 3: The Intersection of the Exit Pupil and Entrance Pupil Shadow

From simple geometry this ratio is

$$\frac{a_x}{A_{R_e}} = 1 - \frac{2\theta}{\pi} - \frac{2x}{\pi R_e}\sqrt{1 - \frac{x^2}{R_e^2}}$$

or

$$\frac{a_x}{A_{R_e}} = 1 - \frac{2}{\pi}\sin^{-1}\frac{x}{R_e} - \frac{2x}{\pi R_e}\sqrt{1 - \frac{x^2}{R_e^2}} \qquad (3)$$

Since R_e is proportional to the resolution radius R (Figure 1), equation (3) can be used to relate the response at the focal plane by using x/R as the variable.

Thus the count rate from a unit point source located at the focal point is

$$S_p = \frac{\pi d_e^2}{4(F+T)^2} N_{eff}$$

or in terms of R, the resolution radius, S_p becomes

$$S_p = \frac{\pi R^2 T^2}{4 F^2 (F+T)^2} N_{eff}. \qquad (4)$$

The response to a plane source which contains one unit of activity per unit area can be obtained by integrating the product of equation (3) and equation (4) over the variable x from 0 to R.

$$dS_a = \frac{\pi R^2 T^2 N_{eff}}{4 F^2 (F+T)^2} \; 2 \pi x \, dx \left(1 - \frac{2}{\pi} \sin^{-1} \frac{x}{R} - \frac{2x}{\pi R} \sqrt{1 - \frac{x^2}{R^2}}\right)$$

or

$$S_a = \frac{\pi^2 R^4 T^2 N_{eff}}{2 F^2 (F+T)^2} \int_0^1 \left(1 - \frac{2}{\pi} \sin^{-1} x - \frac{2}{\pi} x \sqrt{1 - x^2}\right) x \, dx.$$

It can be shown that the integral part equates to 0.125, thus

$$S_a = \frac{k_a R^4 T^2 N_{eff}}{F^2 (F+T)^2} \quad \text{where } k_a = 0.0625 \, \pi^2. \qquad (5)$$

Thus the response to a thin volume distribution is proportional to the resolution radius to the 4th power (R^4). The R^2 response to a point source and the R^4 response to a plane source (plane radius greater than R) are frequently used in the design of collimators.

An interesting result is obtained by assuming a spherical source of unit volume concentration whose radius coincides with the resolution radius R. Using the lateral distribution function

$$1 - \frac{2}{\pi} \sin^{-1} \frac{x}{R} - \frac{2x}{\pi R} \sqrt{\left(1 - \frac{x^2}{R^2}\right)} \quad ,$$

the point distribution function

$$\frac{\pi R^2 T^2}{4 F^2 (F+T)^2} N_{eff} \, ,$$

and noting that thickness of the spherical source at x is $2\sqrt{R^2 - x^2}$, then

$$S_v = \frac{\pi R^2 T^2 N_{eff}}{4 F^2 (F+T)^2} \int_0^R 4\pi x\, dx \left(1 - \frac{2}{\pi} \sin^{-1} \frac{x}{R} - \frac{2x}{\pi R} \sqrt{1 - \frac{x^2}{R^2}}\right) \left(\sqrt{R^2 - x^2}\right)$$

or

$$S_v = \frac{\pi^2 R^5 T^2 N_{eff}}{F^2 (F+T)^2} \int_0^1 \left(1 - \frac{2}{\pi} \sin^{-1} x - \frac{2}{\pi} x \sqrt{1-x^2}\right)\left(\sqrt{1-x^2}\right) x\, dx$$

The integral can be evaluated and equals 0.107

or

$$S_v = \frac{k_v R^5 T^2 N_{eff}}{F^2 (F+T)^2} \qquad \text{where } k_v = 0.107\ \pi^2. \tag{6}$$

Equation (6) indicates that the sensitivity depends on R^5 rather than on R^4. If it is logical to assume that the defects to be found by scanning are more likely to be spherical than planar, then equation (6) would be more applicable in design than equation (5).

Effect of Vertical Displacement on Sensitivity

Figure 4 illustrates the geometry assumed in the derivation of the response from a vertical displacement of a plane source (radius $\cong R'$) located z distance from the focal plane. $(d + 2R')$ is essentially the diameter over which the channels are uniformly distributed.

An approximation to the vertical response may be made by computing the ratio of the resolution area $(\pi R'^2)$ to the total area $\pi(d/2 + R')^2$ at z.

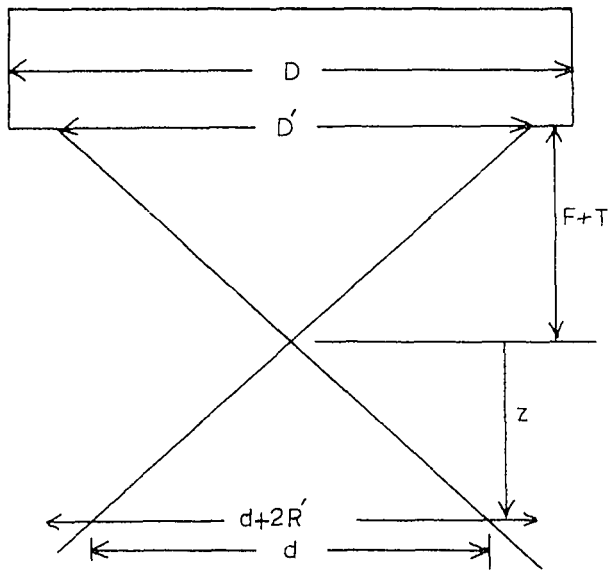

Figure 4: Geometry for Vertical Displacement of Source

This ratio is:

$$\frac{a}{A} = \frac{R'^2}{\left(\frac{z\ D'}{2(F+T)} + R'\right)^2} \quad \text{for z greater than 0,}$$

$$= \frac{1}{\left(\frac{z\ D'}{2R'(F+T)} + 1\right)^2} \qquad \cong \frac{1}{\left(\frac{z\ D'}{2R(F+T)} + 1\right)^2} .$$

Where R = resolution radius at the focal plane

D'= diameter of collimator at crystal surface over which holes are spread

F = focal length

T = collimator thickness

The term $D'^2/4R^2(F+T)^2$ is responsible for the rapid decrease in sensitivity and for comparative purposes is hereby called "Fall Off

Coefficient" (FOC).

From the terms involved the FOC is entirely based on geometry and collimator design. For large z, the function R'(z) approaches a constant times z which would negate the z^2 variation, however at this value of z the term a/A has reached an insignificant value. Small Fall Off Coefficients are desirable for large volume scanning, however it is obvious that small FOCs are not compatible with large sensitivities. Therefore another compromise is necessary in collimator design.

Scanning Speed, Detectability, and Resolution

Equations (4), (5), and (6) can be used to determine the counting rate when the scanner is stationary and over one of the source distributions previously described (point, plane, volume). In actual use the scanner is in motion and records, within statistical limitations, the planar distribution of radioactivity.

With the exception of the point source distribution, the change in counting rate as the scanner moves across the defect is somewhat cumbersome to handle mathematically. For this reason, two approximations will be used to derive the interparameter relationships.

Straight Line Approximation

For this case the counting rate is assumed to be C_o when the scanner is displaced R units from the peak counting rate (C_m+C_o), and approaches C_m+C_o as a linear function of time. Thus, $C_t = C_o + ktC_m - C_o = kC_m t$.

Figure 5 illustrates the type of function assumed. R is the resolution radius as previously described.

If the scanner were stationary over C_m for τ minutes and then

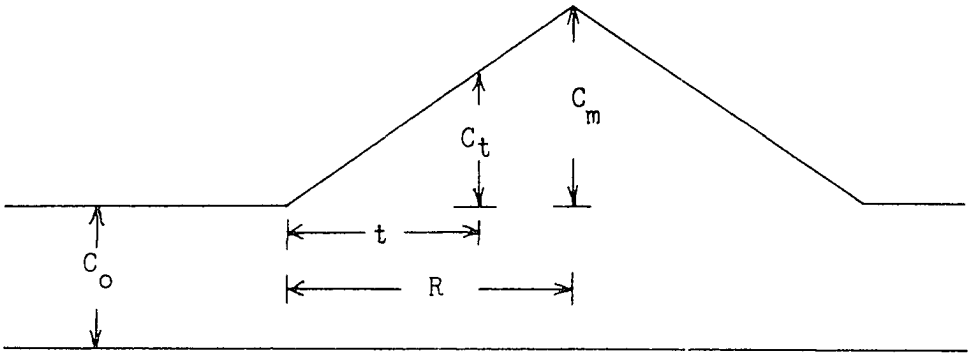

Figure 5: The Linear Approximation

moved to C_o for γ minutes, the resulting count differential would be

$$C_m\gamma \left(1 \pm \sqrt{\frac{2\,C_o\gamma + C_m\gamma}{C_m^{\,2}\,\gamma^{\,2}}}\right)$$

or

$$C_m\gamma \left(1 \pm \sqrt{\frac{2\,C_o\gamma}{C_m^{\,2}\,\gamma^{\,2}}}\right) \text{ for } C_m \text{ much less than } C_o.$$

As in any counting problem the certainty of C_m is entirely determined by

$$\frac{2\,C_o\gamma}{C_m^{\,2}\,\gamma^{\,2}} = (\text{fractional deviation})^2 = (fd)^2.$$

Therefore the parameters which minimize $(fd)^2$ are the ones being sought.

Since the scanner is in motion in the actual case, the preceeding equation for $(fd)^2$ cannot be used. The solution is straight forward by letting

S = scanning speed

γ = integration or time constant of the recording electronics

N = number of independent counting intervals in R

R = resolution radius.

Then

$$C_t = \frac{C_m S t}{R}$$

$$\text{Counts in } \gamma = \int_{(n-1)\gamma}^{n\gamma} C_m \frac{S}{R} t \, dt \quad \text{where } n = 1,2, \text{ up to N,}$$

or

$$\text{Counts/Interval} = \frac{C_m S}{2R} (2n-1)\gamma^2. \quad \text{This is a maximum when}$$

n = N, therefore

$$\text{Counts/Interval} = \frac{C_m S}{2R} (2N-1)\gamma^2, \text{ and}$$

$$(fd)^2 = \frac{2 C_o 4 R^2 \gamma}{C_m^2 S^2 (2N-1)\gamma^4}, \text{ since } N\gamma = R/S \text{ or } \gamma = R/NS, \text{ and}$$

$$(fd)^2 = \frac{8 C_o}{C_m^2} \frac{N^2}{(2N-1)^2 \gamma}. \tag{7}$$

Equation (7) states that γ shall be large and that N should exceed 3. However, since N, T, and S are related, equation (7) can be stated without the γ dependence.

$$(fd)^2 = \frac{8 C_o N^3 S}{C_m^2 (2N-1)^2 R}. \tag{8}$$

If C_o is determined for a uniform volume distribution, and C_m determined for a point source distribution, equations (7) and (8) can be used to obtain

$$(fd)^2 = \frac{8 k_a K_a T_o R^4 N^3 S c_o}{k_p^2 K_a^2 R^4 (2N-1)^2 R c_v^2 V_t^2}$$

or

$$(fd)^2 = \frac{8\, k_a\, T_o\, N^3\, S\, c_o}{k_p^{\,2}\, K_a\, (2N-1)^2\, R\, c_v^{\,2}\, V_t^{\,2}} \qquad (9)$$

where $k_a = 0.0625\ \Pi^2$

$k_p = \Pi/4 = 0.25\ \Pi$

$$K_a = \frac{T^2}{F^2\,(F+T)^2}\ N_{eff}$$

T_o = thickness of NON-tumor part

c_o = volume concentration NON-tumor

c_v = differential volume concentration of tumor

V_t = volume of tumor.

The dimensions of the tumor volume V_t should be small compared to R since the point source distribution was used. Equation (9) does not include the effect of absorption and scatter. Although $N^3/(2N-1)^2$ reaches a minimum at N = 1.5, it does not change significantly until N is greater than 3. Thus, even for point sources, the best detectability is associated with large R. On the other hand, if the shape of the defect is required, then R will have to be made as small as necessary since the spatial resolving ability cannot be less than R. One point of interest is that τ is completely determined if S and N are fixed--$\tau = R/NS$.

For defects or tumors whose dimensions are of the order of R, or larger, the scanner will begin detecting counts from the defect at a displacement of 2R rather than R as assumed in equations (7) and (8).

The preceeding derivations may be modified to include this effect by changing the parameters--N to 2N and R to 2R, where τ is still the integration time and N is the number of independent samples in R, or 2N is the number of independent samples in 2R.

Equation (7) then becomes

$$(fd)^2 = \frac{8\,C_o}{C_m^{\,2}} \quad \frac{(2N)^2}{(4N-1)^2\,\gamma} \tag{10}$$

and equation (8) becomes

$$(fd)^2 = \frac{32\,C_o}{C_m^{\,2}\,R} \quad \frac{N^3\,S}{(4N-1)^2} \tag{11}$$

The minimum is at N = .75 instead of 1.5 as before. Using the uniform surface response for C_o and C_m where the defect is of radius R, equation (8) becomes

$$(fd)^2 = \frac{32\,T_o\,N^3\,S\,c_o}{k_a\,K_a\,c_v^{\,2}\,T_v^{\,2}\,R^5\,(4N-1)^2} \tag{12}$$

where T_o = non-tumor thickness

c_o = non-tumor concentration

c_v = differential tumor concentration

T_v = tumor thickness

R = resolution radius and tumor radius .

Using a spherical tumor of radius R, equation (8) becomes

$$(fd)^2 = \frac{32\,k_a\,T_o\,N^3\,S\,c_o}{k_v^{\,2}\,K_a\,c_v^{\,2}\,R^7\,(4N-1)^2}. \tag{13}$$

For defects which are large compared to the resolution radius R, there is a region of essentially constant count rate over the defect. The linear approximation is of no value in minimizing $(fd)^2$ and one may as well use the expression

$$(fd)^2 = \frac{2\,C_o\,\gamma}{C_m^{\,2}\,\gamma^2} = \frac{2\,C_o}{C_m^{\,2}\,\gamma} \tag{14}$$

using the uniform surface response functions for C_o and C_m. After substituting, equation (14) becomes

$$(fd)^2 = \frac{2\ T_o\ c_o}{k_a\ K_a\ c_v^{\,2}\ T_v^{\,2}\ R^4\ \gamma} \tag{15}$$

$$(fd)^2 = \frac{2\ T_o\ c_o\ S}{k_a\ K_a\ c_v^{\,2}\ T_v^{\,2}\ R^4} \quad \frac{N_T}{R_T} \tag{16}$$

where R_T is the tumor radius

and N_T is the number of independent counting intervals in R_T. If the location of the tumor edge is to be determined within $\pm$ R, then γ will have to be R/S or perhaps R/2S, in which case equation (16) becomes

$$(fd)^2 = \frac{4\ T_o\ c_o\ S}{k_a\ K_a\ c_v^{\,2}\ T_v^{\,2}\ R^5} \tag{17}$$

where R is much less than R_T.

Summary of Linear Approximation.

1. Small defects in large pool of radioactivity:

$$(fd)^2 = \text{proportional to } \frac{S}{R}\ \frac{N^3}{(2N-1)^2}\ .$$

2. Cylindrical defects (R_T = R) in large pool of radioactivity:

$$(fd)^2 = \text{proportional to } \frac{S}{R^5}\ \frac{N^3}{(4N-1)^2}\ .$$

3. Spherical defects R_T = R in large pool of radioactivity:

$$(fd)^2 = \text{proportional to } \frac{S}{R^7}\ \frac{N^3}{(4N-1)^2}\ .$$

Quadratic Approximation

For defects of the same order of size as the resolution radius, the linear approximation shape at the maximum counting rate C_m is probably inadequate.

A quadratic approximation in which the change in counting rate may be represented by $C_t = k_1 t - k_2 t^2$ is illustrated in Figure 6.

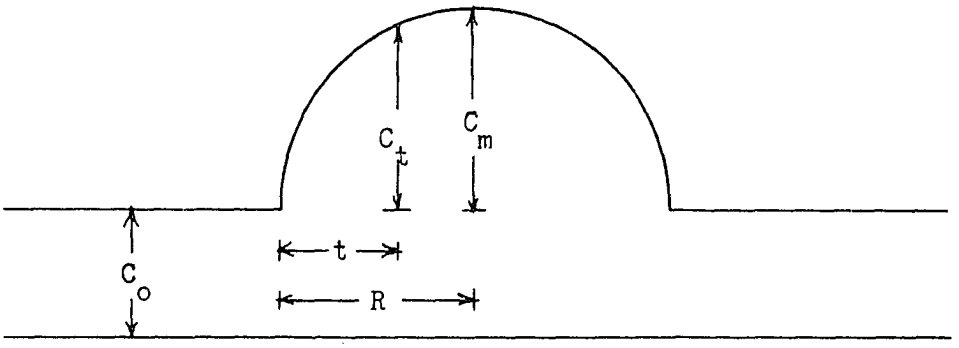

Figure 6: The Quadratic Approximation

Using the same variables as before, the following is obtained:

$$C_t = C_m \left(\frac{2 S t}{R} - \frac{S^2 t^2}{R^2}\right)$$

$$\text{and counts in } \gamma = C_m \left[\frac{S t^2}{R} - \frac{S^2 t^3}{3 R^2}\right]_{(N-1)\gamma}^{N\gamma}$$

$$= C_m \left[\frac{S}{R}(2N-1)\gamma^2 - \frac{S^2\gamma^3}{3 R^2}(3N^2 - 3N + 1)\right] .$$

After substituting $S = \frac{R}{\gamma N}$

$$\text{counts in } \gamma = C_m \frac{\gamma}{3 N^2}(3N^2 - 1)$$

$$\text{and } (fd)^2 = \frac{18\, C_o\, N^4}{C_m^{\,2}\, \gamma\, (3N^2 - 1)^2} .$$

In terms of S

$$(fd)^2 = \frac{18\, C_o\, N^5\, S}{C_m^{\,2}\, R\, (3N^2 - 1)^2} . \qquad (18)$$

This reaches a minimum at N = 1.3 although the value is almost identical at N = 1, 2, or 3.

As in the linear case, the variables N and R are changed to include the fact that the scanner is able to detect defect counts at displacements 2R. As before, N is changed to 2N and R is changed to 2R, and equation (18) becomes

$$(fd)^2 = \frac{288\, C_o\, S\, N^5}{C_m^{\,2}\, R\, (12N^2 - 1)^2} . \qquad (19)$$

Using the various substitutions for C_o and C_m we have for the quadratic approximations:

1. Cylindrical defects ($R_t = R$) in a large radioactive pool:

$$(fd)^2 = \text{proportional to } \frac{N^5}{(12N^2 - 1)^2} \frac{S}{R^5} .$$

2. Spherical defects ($R_t = R$) in a large radioactive pool:

$$(fd)^2 = \text{proportional to } \frac{N^5}{(12N^2 - 1)^2} \frac{S}{R^7} .$$

Where S is scanning speed, N is the number of independent samples in R, and R is the resolution radius. It is apparent that the linear and quadratic approximations are identical in S and R terms.

Dot Factors and Mechanical Printers

Most of the commercial scanners have a mechanical stylus which prints a dot or hash mark for each impulse received. This marker moves with the scanning head so that there is a one to one spatial relationship between the scanning head and marker. Due to the limited rate at which the marker can print, there is a scaling circuit between the detector and marker which divides the number of incoming pulses by some factor before they actuate the marker. This factor is called the dot factor.

Since the marker is not actuated until K (dot factor) pulses are received, the dot factor, in a sense, determines the integration time. Unlike the fixed integration time γ in the preceeding linear approximation derivations, the dot factor produces a variable time constant which is inversely proportional to the total counting rate. Since the printer prints one mark for every K counts

$$\gamma(t) = \frac{K}{\text{Average counts/minute over the interval}} .$$

Using the linear approximation and dividing the interval R/S into N unequal segments, it can be shown that

$$\gamma_n \left[2N\, C_o + C_m\, (2n-1) \right] = 2NK$$

or

$$\gamma_n = \frac{K}{C_o + C_m \frac{2n-1}{2N}} \qquad \text{where n is the nth interval.}$$

During this time γ_n the detector will have detected K counts, some of which are due to the defect, and some due to the radioactive pool surrounding the defect. When C_m/C_o is very small γ_n can be expanded into a linear equation:

$$\gamma_n = \frac{K}{C_o} \frac{1}{1 + \frac{C_m}{C_o} \frac{(2n-1)}{2N}}$$

$$= \frac{K}{C_o} \left(1 - \frac{C_m}{C_o} \frac{2n-1}{2N} \right) .$$

Since there are K counts in this interval $K - C_o \gamma_n$ = counts due to defect or

$$\text{counts due to defect} = \frac{K C_m}{C_o} \frac{2n-1}{2N},$$

and

$$(fd)^2 = \frac{2 C_o \gamma_n}{\left[\frac{K C_m}{C_o} \frac{(2n-1)}{2N}\right]^2}$$

$$(fd)^2 = \frac{2 C_o^2 \left(1 - \frac{C_m}{C_o} \frac{(2n-1)}{2N} \right)}{K C_m^2} \frac{4 N^2}{(2n-1)^2}$$

$$(fd)^2 = \frac{2 C_o^2}{K C_m^2} \frac{4N^2}{(2n-1)^2}$$

This reaches a minimum at n = N so

$$(fd)^2 = \frac{2 C_o^2}{K C_m^2} \frac{4 N^2}{(2N-1)^2} .$$

This is identical in form to the linear approximation for fixed γ and leads to the same result if $N\gamma = R/S$ and $NK/C_o = R/S$.

For $K = R C_o/NS$

$$(fd)^2 = \frac{2 C_o S}{C_m^2 R} \frac{4N^3}{(2N-1)^2}$$

which is identical to equation (8) for point source linear approximation. The extenxion to range 2R is carried out as before producing

$$(fd)^2 = \frac{32\ C_o}{C_m^{\ 2}\ R} \quad \frac{S\ N^3}{(4N-1)^2} \qquad \text{for defects of radius R.}$$

The main difference between dot factor integration and sequential time integration is the increase of γ_n when $C_o + C_m(t)$ decreases for a fixed K. This increases the time constant and may produce an impulse to the printer at a delayed time far removed from the site which produced the counts. This effect is called "Scalloping".

Most of the commercial scanners use the dot factor type of integration although it is not as flexible as an independently adjustable integration time constant would be.

Photo Recorder

In addition to the mechanical or "dot" printer, there is usually a photographic system coupled to the scanning unit which converts pulses from the detector to light quanta and records these on photographic emulsion. While the statistics are the same, the photo recorder has a much faster resolving time, therefore it does not require a dot factor device. The photo recorder also has a certain amount of contrast, or non linear amplification, due to the film emulsion characteristics. If additional non linear amplification is desired, various electronic circuits are available which increase either or both the light intensity and the light pulse duration, thus causing a more sifnificant impression on the film. The inherent danger in these high contrast techniques is that expected normal statistical variations may produce false defects

on the photo scan.

Since both photo and dot scans are produced from the same statistical information, one should not be more accurate than the other. The differences in interpretation, however, eventually involve the human eye wherein individual preferences determine which scan is the more useful.

The Effect of Scattering on Detectability

In the preceeding sections it was assumed that the photons or gamma rays retained their initial isotropic distribution. Due to the various scattering and absorption processes, the initial distribution of emitted photons will change, both in spatial distribution and in energy distribution. Therefore, the detector will record an energy spectrum which will be different from the source spectrum even though the medium surrounding the source contains the same radioisotope.

It is convenient to assume a distribution having a single photo peak and a single channel pulse height analyzer with an adjustable window. If $\int_{E}^{E_{max}} S_E \, dE$ is the number of counts from the source proper and $\int_{E}^{E_{max}} N_E \, dE$ is the number of counts from non-source origin, then

$$(fd)^2 = \frac{\int_{E}^{E_{max}} 2 \, N_E \, dE}{\left(\int_{E}^{E_{max}} S_E \, dE \right)^2} \quad (\text{for } N_E \gg S_E) \tag{20}$$

is a function of E, where

N_E = number of photons per unit energy interval of non-source origin

S_E = number of photons per unit energy interval from source origin

E_{max} = spectrum end point.

Equation (20) can be differentiated with respect to E and the result equated to 0 to obtain

$$\frac{N_E}{S_E} = \frac{2\int_E^{E_{max}} N_E \, dE}{\int_E^{E_{max}} S_E \, dE} . \qquad (21)$$

Obviously if N_E has the same spectral shape as S_E, no minimum exists and $(fd)^2$ would have the smallest value at E=0. If on the other hand N_E differs from S_E (the usual case), there may exist an E such that equation (21) is satisfied. At this E the $(fd)^2$ is a minimum even though some (or most) of the spectrum is discarded.

The integrals in equation (21) cannot be evaluated in closed form because no single mathematical expression exists for N_E and S_E. Both are functions of defect size, shape, and depth, as well as the shape and volume of the non defect radioisotope distribution.

Some approximations can be made however, for conditions such that N_E and S_E have identical shapes between E_{max} and E_1, where E_1 is smaller than the photopeak E_p. Over this range $N_E=KS_E$ and the ratio of the integrals in equation (21) has the value K. If N_E at $E=E_1$ deviates from S_E in a short interval of E, then

$$(fd)^2 = \text{minimum at E such that } N_E = 2KS_E . \qquad (22)$$

Even the approximation of equation (22) cannot be used unless N_E and S_E are known spectra. They cannot be determined from the clinical scanning procedure since the detector records both simultaneously. A common procedure is to determine S_E from a source in air, and N_E from a

plastic or water phantom filled with a radioactive solutions. Neither of these is ideal.

When the spectrum of N_E differs in shape from that of S_E at E values greater than the photopeak energy E_p, equation (21) is still valid but must be solved graphically.

Equation (21) results in the minimum $(fd)^2$ for determining the existence of a defect. Under certain conditions it is desirable to maximize the difference between count rate at the defect center and the count rate at the defect edge. This could also be called maximizing the shape factor. If $S_E = 0$ at the defect edge, equation (21) applies directly. However, if due to scatter or other reasons, part of S_E is still detected, equation (21) can be modified to yield the minimum $(fd)^2$ for the shape factor. Since N_E does not change, equation (21) becomes

$$\frac{N_E}{S_{OE} - S_{XE}} = \frac{2\int_E^{E_{max}} N_E \, dE}{\int_E^{E_{max}} (S_{OE} - S_{XE}) \, dE}$$

where S_{OE} = spectrum of source at defect center

S_{XE} = spectrum of source where scanner is displaced X centimeters from defect center.

X is arbitrary and will depend on how much sharpness is desired, recognizing that as X approaches 0 -----$(fd)^2$ approaches infinity.

CHAPTER III

EXPERIMENTAL PROCEDURE

A very important factor in deciding the experimental procedures was the fact that all of the scanners involved were in clinical use and would not be available for the usual laboratory type studies. Thus, the experimental apparatus would of necessity have to be dismantled each night so that the routine clinical studies could proceed the following day. Therefore, the experimental apparatus would have to be portable and reasonably simple to transport.

Another factor was the desirability to use a range of gamma energies which spanned the energies routinely used in clinical scanning. For this reason, 4 radioisotopes were selected:

1. Hg-197, E = 77 KV
2. Co-57, E = 122 KV
3. Hg-203, E = 279 KV + ----
4. I-131, E = 364 KV + ---- .

Au-198 would also have been selected except for its short half life. It is reasonable to assume that the difference between Au-198 and I-131 could be obtained by extrapolation and inference from the I-131 data. The half life of Hg-197 is not very satisfactory for an extended experimental procedure, however it was considered desirable to include at least one energy in this range.

The available specific activities of the selected isotopes precluded the use of point sources. Therefore, volume sources were used.

Although any number of source volumes could be used satisfactorily, a cylindrical volume 12 mm in height and 12 mm in diameter was used for all sources. With the exception of Co-57, the source radioisotopes are routinely available at most scanner installations. The Co-57 source (5 uc) was donated by Abbott Laboratories.

A source holder consisting of several sheets of plexiglass was constructed so that the test source could be effectively moved in all three dimensions. Plastic was used instead of water because of easier dismantling and portability. The slight increase in density and the slightly fewer electrons per gram were not considered objectionable. The overall dimensions of the source holder (phantom) were 6.5 inches by 6.5 inches by 6.5 inches. The plexiglass sheet thickness varied from 1/16 inch to 1 inch; the 1 inch sheet being divided into thirds. The source was imbedded in the central third of the 1 inch sheet to allow movement of the source parallel to the sheet plane. Vertical movement was achieved by transferring sheets from top to bottom, thus changing the source-edge distance. Lateral motion perpendicular to the motion of the divided sheet was accomplished by moving the scanning head.

The detected gamma photons were recorded by a 100 channel Technical Measurements Corporation Analyzer. The analyzer with its high impedance amplifier was electrically wired to the phototube(s) preamplifier. There was no appreciable effect of the TMC analyzer on the scanner electronics. The photopeaks were found at the same scanner analyzer settings with or without the TMC analyzer connected. After a suitable warm-up time

(approximately 30 minutes), the 100 channel analyzer gain was adjusted so that channel 100 corresponded to 500 KV.

The quantity of radioactivity, with the exception of Co-57, was adjusted to produce approximately 10,000 counts per channel per minute at the photopeak with the most efficient collimator available.

Spectra were determined at each 2 millimeters of source displacement using the live time selector of the 100 channel analyzer to compensate for coincidence losses.

The live time selector was initally set to produce a total of 10,000 to 100,000 counts per channel. As the count rate reduced, due to the source displacement, the counting time was increased to produce data which would have a very small statistical spread.

The data from the distribution measurements was plotted on a 3 cycle semilog paper to allow the large ratios of counting rates to be presented on the same graph. The data from each channel was plotted against millimeters displacement to indicate the very striking changes in spectral distribution which take place.

The physical parameters of each collimator were measured with a vernier micrometer which has an error of $\pm$ .001 inch although this precision was not necessary since the parameters themselves had variations in excess of .01 inch.

To simulate the background or non-tumor activity usually found in practical scanning applications a plastic "Purex" bottle approximately 6.5 inches in diameter was filled to a depth of 6.5 inches with a solution of water and the radioisotope being used. Spectra were obtained for each isotope used (except Co-57), and the results plotted on semilog

paper. The normalizations of such plots were carried out in a straight forward manner.

CHAPTER IV

ANALYSIS OF RESULTS

As mentioned in the preceeding section on theory, there are several parameters involved which are fixed by the manufacturer. Focal length, collimator thickness, hole diameters, number of collimator holes, electronic accessories, etc, are examples of these. With the exception of a fixed window (14 percent) in the pulse height analyzer of the Nuclear-Chicago Pho Dot scanner, the electronics of all 4 scanners are very similar. Therefore, no electronic comparisons were made.

The collimators, on the other hand, do differ in design and to illustrate their differences each of the parameters which are involved in the theory were determined by physical measurement, or from the manufacturers literature. Table 1 shows these values where F, T, D, D', N and de are measured dimensions and f, R, N_{eff}, K_a, and FOC are computed values, using the relationships developed in the preceeding chapter. It is apparent that the manufacturers were designing for a similar resolution radius (R), particularly for the large hole collimators.

If one were interested in finding defects only at the focal plane, the scanner with the largest K_aR^n (where n depends on the type of response function--point, cylindrical, or spherical) would be selected. For reasons already outlined, a large K_a is also associated with a large Fall Off Coefficient (FOC) which reduces the scanner sensitivity at points

TABLE I

COMPARISON OF COLLIMATOR PARAMETERS

SCANNER	D	D'	d_e	F	T	R	N_{eff}	f	FOC	K_a
	inches	inches	inches	inches	inches	cm			in^{-2}	in^{-2}
Picker 3"										
19 Hole	3	2.5	.475	3	3	1.21	18.7	.68	.193	.52
31 Hole	3	2.5	.3	3	4	.57	30.5	.44	.63	1.1
Nuclear-Chicago Pho Dot										
19 Hole	3	2.95	.495	2.68	3	1.12	18.4	.54	.35	.71
37 Hole	3	2.86	.308	2.48	3.05	.64	36	.43	1.04	1.72
61 Hole	3	3	.242*	2.28	3.1	.46	58.5	.40	2.38	3.69
Ohio Nuclear										
199 Hole	8	7.125	.365	3.5	2.61	1.25	165	.52	1.4	2.47
253 Hole	8	7.125	.338	3.5	3.275	.92	218	.57	2.1	4.16
Picker 5"										
5 BF 85 Hole	5	4.875	.325*	5	3.35	1.24	81	.38	.36	.52
5 FF 265 Hole	5	4.875	.175*	5	3.35	.665	254	.34	1.12	1.70
3 BF 31 Hole	5	4.875	.593*	3	3.35	1.35	28.7	.47	.72	.89
3 FF 163 Hole	5	4.875	.242*	3	3.35	.55	151	.40	3.16	4.68

* d_e^* = 1.05 w for hexagonal holes
where w = interface width

TABLE II

COMPARISON OF SCANNER SENSITIVITIES

SCANNER	R	K_aR^2	K_aR^4	K_aR^5	FOC
	Inches	Point Response	Surface Response	Spherical Response	$Inches^{-2}$
Picker 3"					
19 Hole	.475	.118	.0265	.0126	.193
31 Hole	.225	.056	.00286	.00063	.63
Nuclear-Chicago Pho Dot					
19 Hole	.438	.136	.0262	.0115	.35
37 Hole	.252	.110	.0069	.00176	1.04
61 Hole	.181	.121	.00395	.000715	2.38
Ohio Nuclear					
199 Hole	.49	.59	.142	.0695	1.4
253 Hole	.363	.55	.072	.0262	2.1
Picker 5"					
5 BF 85 Hole	.486	.123	.029	.014	.36
5 FF 265 Hole	.262	.117	.008	.0021	1.12
3 BF 31 Hole	.532	.252	.071	.038	.72
3 FF 163 Hole	.216	.22	.0102	.0022	3.16

not on the focal plane.

The fraction of the crystal which is exposed is given by the factor f. Sensitivity increases directly with f, however so does leakage or septa penetration. No significant leakage was observed for energies up to 280 KeV. There was detectable septa penetration at 364 KeV, however the effect was small and probably does not reduce the utility of the collimators for energies including 364 KeV.

The experimental determination of R was calculated from the shape of the measured distribution curves of counts per channel versus source displacement. It was assumed that the test source (12 mm) would behave, at some distance--lateral to the focal point, like a point source and that the gaussian approximation of Brownell[2] would provide a suitable technique for the determination of R. Brownell's approximation to a point source distribution is

$$Y = Y_o \, e^{-2.78 \frac{X^2}{R^2}}$$

where R is the resolution radius and X is the source displacement. It can be shown that

$$R = \frac{-2.43}{\text{slope } (\log Y)} \qquad (23)$$

if the slope is determined at $Y = 0.062\ Y_o$. Since the counts per channel are plotted on semilog paper, equation (23) is simple to use.

Figures 7 and 8 represent typical results for 2 gamma ray energies.

When one attempts to determine the resolution radius by equation (23), a series of values is obtained depending on which channels are used.

If the spectral change is entirely due to Compton scatter, the best estimate of R is the one determined at the channel having the steepest

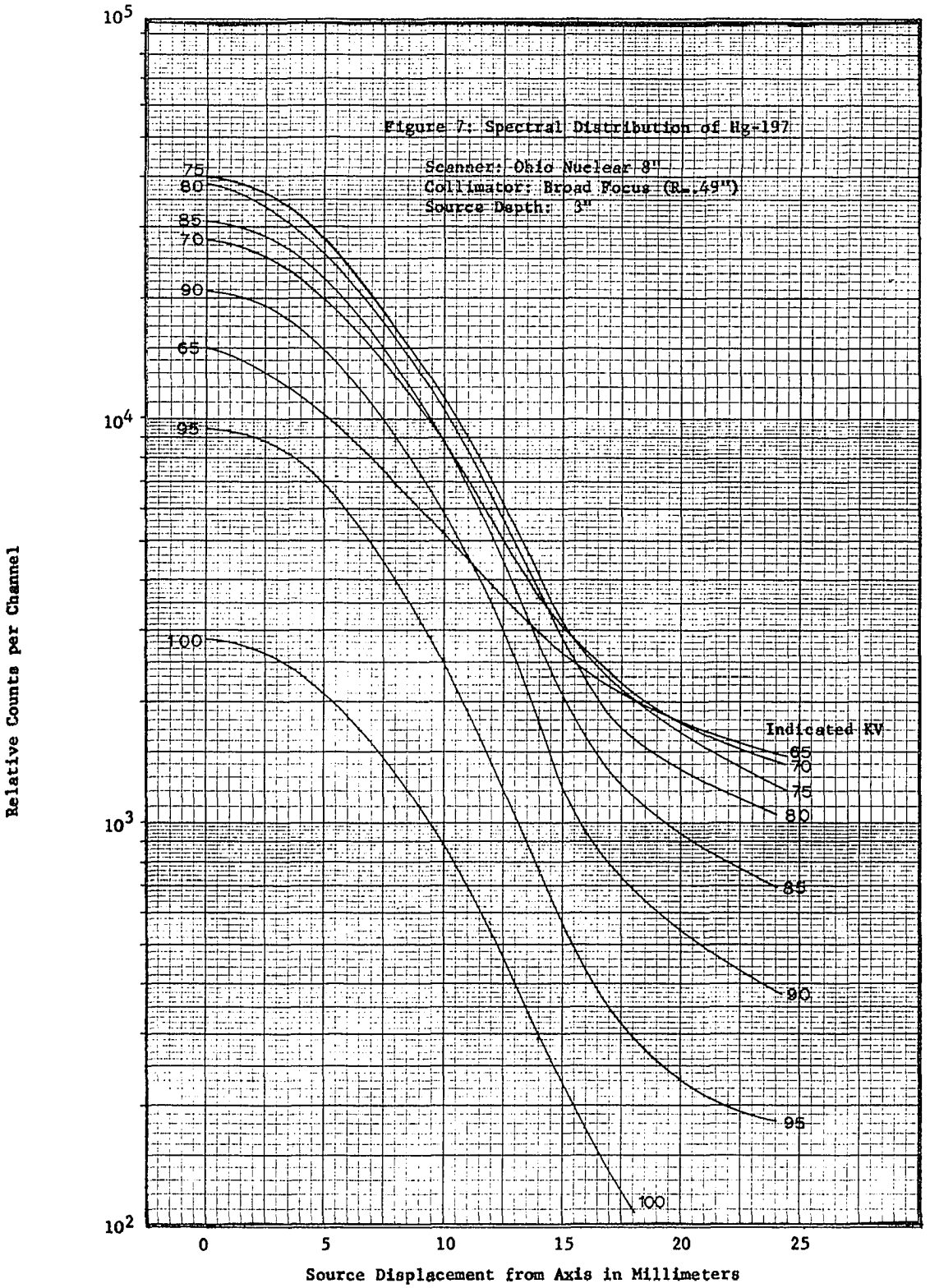
Figure 7: Spectral Distribution of Hg-197
Scanner: Ohio Nuclear 8"
Collimator: Broad Focus (R=.49")
Source Depth: 3"
Relative Counts per Channel
Source Displacement from Axis in Millimeters
Indicated KV
65
70
75
80
85
90
95
100

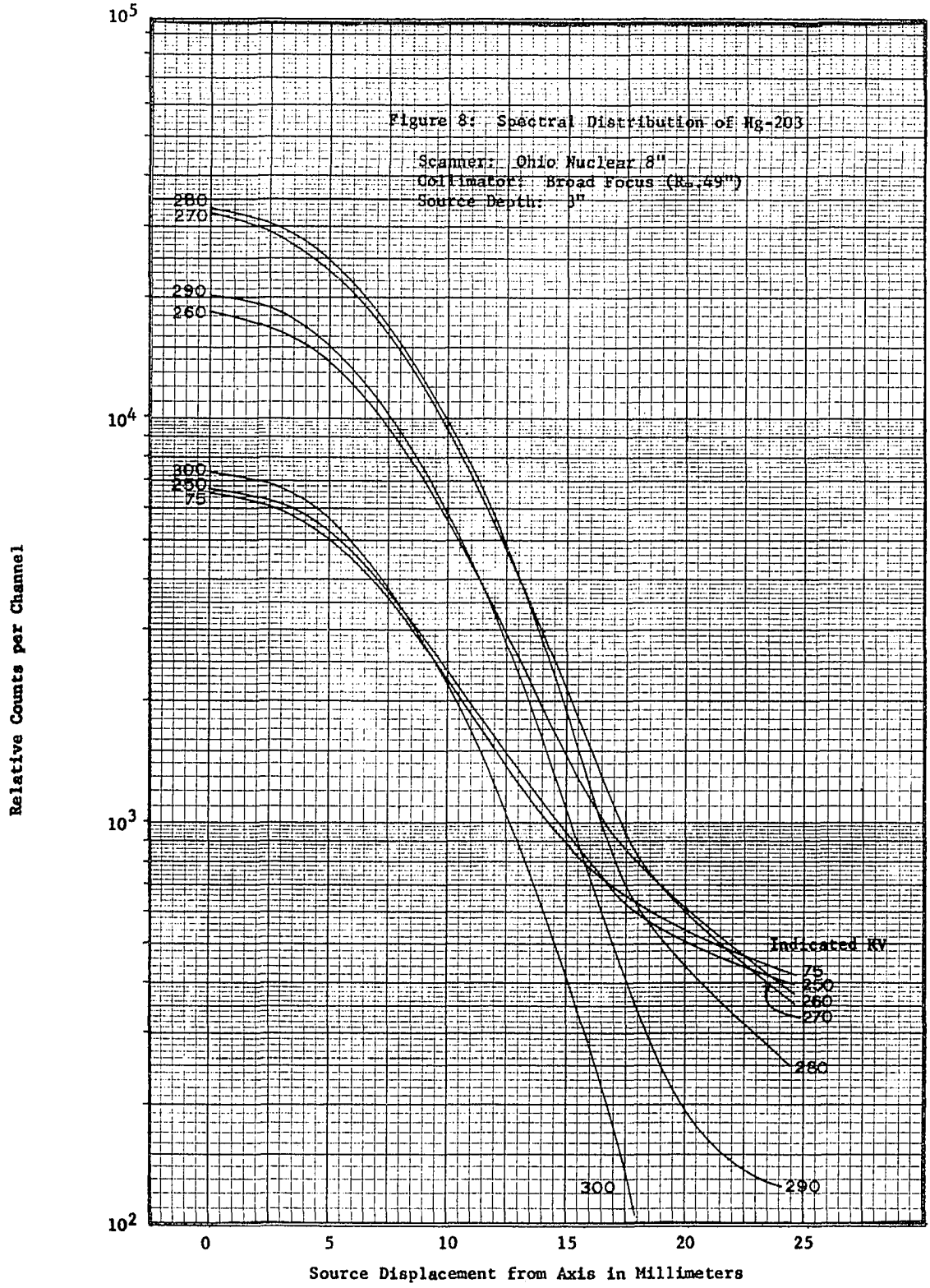
Figure 8: Spectral Distribution of Hg-203
Scanner: Ohio Nuclear 8"
Collimator: Broad Focus (K=.49")
Source Depth: 3"
280
270
290
260
300
250
75
Indicated KV
75
250
260
270
280
290
300
10^5
10^4
10^3
10^2
0
5
10
15
20
25
Relative Counts per Channel
Source Displacement from Axis in Millimeters

slope. When this is done the value of R obtained is approximately 1.25 times the theoretical R for Hg-203 and I-131, and approximately 1.6 times R for Hg-197.

Several other distributions are included in the Appendix. All of the curves however, indicate that the apparent resolution radius increases with decreasing energy. In fact, the shape of the distribution curve is so characteristic of the energy that one can almost identify the isotope by the shape of the curve.

No distribution curves were obtained in air. It would be expected that the apparent resolution would approach R and that the gaussian approximation would more nearly fit the data.

Also included in the Appendix are spectra from the large volume containers (Purex bottles) with either I-131, Hg-203, or Hg-197. (There was insufficient Co-57 available to simulate the large volume scatter for this energy.) The same scattering characteristics are noted in these spectra as in the source distribution curves. Therefore, the window selection for minimum $(fd)^2$ for the low energies (equation 21) will necessitate the discarding of a large fraction of the total photopeak regions. For maximum defect shape, the window threshold may even be required to be greater than the photopeak energy.

The Fall Off Coefficient (FOC) was determined at a vertical source displacement of 2 inches. The values are in agreement with the theoretical values in Table 1 for Hg-203 and I-131 but are slightly greater for Hg-197 and Co-57. This difference is not unexpected since the absorption coefficients (u_a) are greater for these lower energies.

No attempt was made to evaluate the collimators using the optimum

design criteria of Beck[3]. To use Beck's data one must have some design purpose in mind. For the collimators tested, there is no information available concerning the manufacturer's intent nor any information available indicating the reasons for the compromises made.

Whether or not the linear (or quadratic) approximations and the resulting optimal integration times are valid remain to be tested. The theory developed in Chapter II appears logical, however, like all theories it is of no value unless it can be applied to practical clinical scanning.

The shape of the distribution curves for low energy gamma sources indicates a large comparative increase in scatter. While most of the observed spectral changes can be explained on the basis of Compton incoherent scatter, the possibility exists that coherent scatter is appreciable. The separation of coherent from incoherent scattering cannot be carried out with the existing experimental arrangement. This separation probably can be accomplished using higher resolution devices such as the ion drift detectors.

CHAPTER V

CONCLUSION

There is a considerable variation in the sensitivities of scanners, depending on the response used for comparison (Table II). Wide angle systems and small R (high resolution) systems are associated with large fall off effects which reduce the utility of these systems for screening purposes.

The extension of the theory developed in Chapter II and the analysis of the distribution curves lead to the following:

1. The data in this evaluation does not support the popular belief that low energy gamma emitters offer improved scanning possibilities. On the contrary, the data suggests that medium energies (200 - 400 KeV) have greater potential as scanning agents.

2. The data does not support the opinion of some (Blau & Bender)[4] that Hg-203 has significantly better physical characteristics for scanning than I-131.

3. The theoretical derivations suggest that it may be possible to produce improved scans by increasing the resolution radii to values in excess of those in present use, and at the same time using more selective windows. Collectively, due to the R^4 and R^5 terms in sensitivity, these two changes could result in greater sensitivity without appreciable loss in effective resolution.

4. An optimum of window settings could be achieved if the non-defect spectrum N_E were determined from the actual type of organ being scanned. This could be accomplished by using the patients themselves with multichannel analyzers. Spectra could be determined from livers, kidneys, brains, etc. This would allow maximum utilization of the emitted radiations.

5. The existing read-out systems result in data which has no fixed interpretation. A digital numerical system would eliminate one source of error (human) in determining whether a defect was statistically present or not. Digital read-outs would also be more adaptable to electronic data processing. This would not relieve the clinician of his responsibilities in using the results of scans, but would shift the burden of statistical analysis to a more uniform system.

BIBLIOGRAPHY

1. Harris, C. C., "Scanner Collimators", Picker Scintillator, Volume 9, Number 4-C, June 1965.

2. Brownell, G. L., "Resolution of Gamma Imaging Devices", Picker Scintillator, Volume 9, Number 2-C, May 1965.

3. Beck, R. N., "A Theory of Radioisotope Scanning Systems", Proceedings of the Symposium on Medical Radioisotope Scanning, I. A. E. A., 1964.

4. Blau, M. and Bender, M. A., "Radiomercury (Hg-203) Labeled Neohydrin: A New Agent for Brain Tumor Localization", J. Nuclear Medicine, 3: 83-93, 1962.

APPENDIX

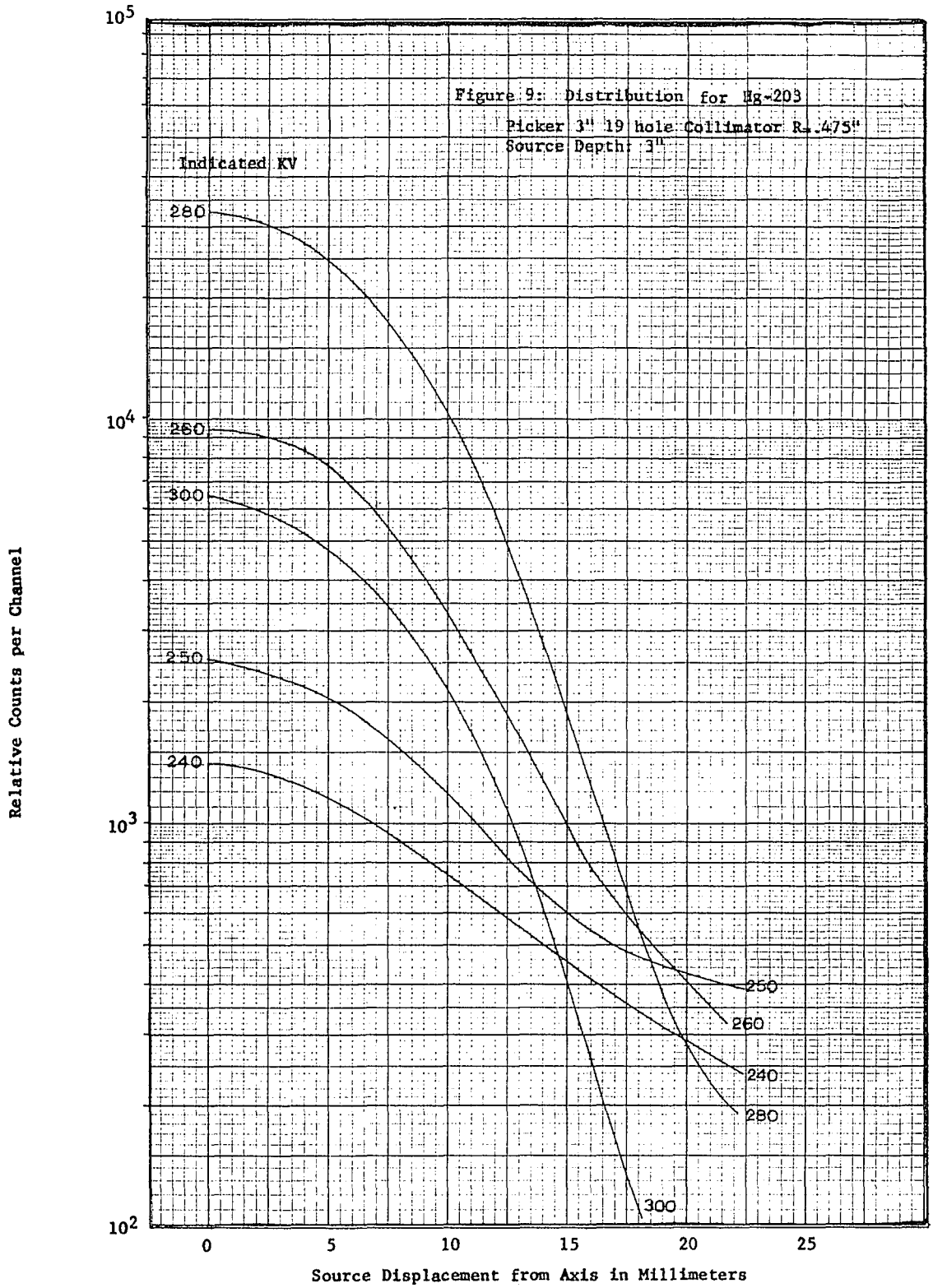
Figure 9: Distribution for Hg-203
Picker 3" 19 hole Collimator R=.475"
Source Depth: 3"
Indicated KV
280
260
300
250
240
10^5
10^4
10^3
10^2
Relative Counts per Channel
0
5
10
15
20
25
Source Displacement from Axis in Millimeters

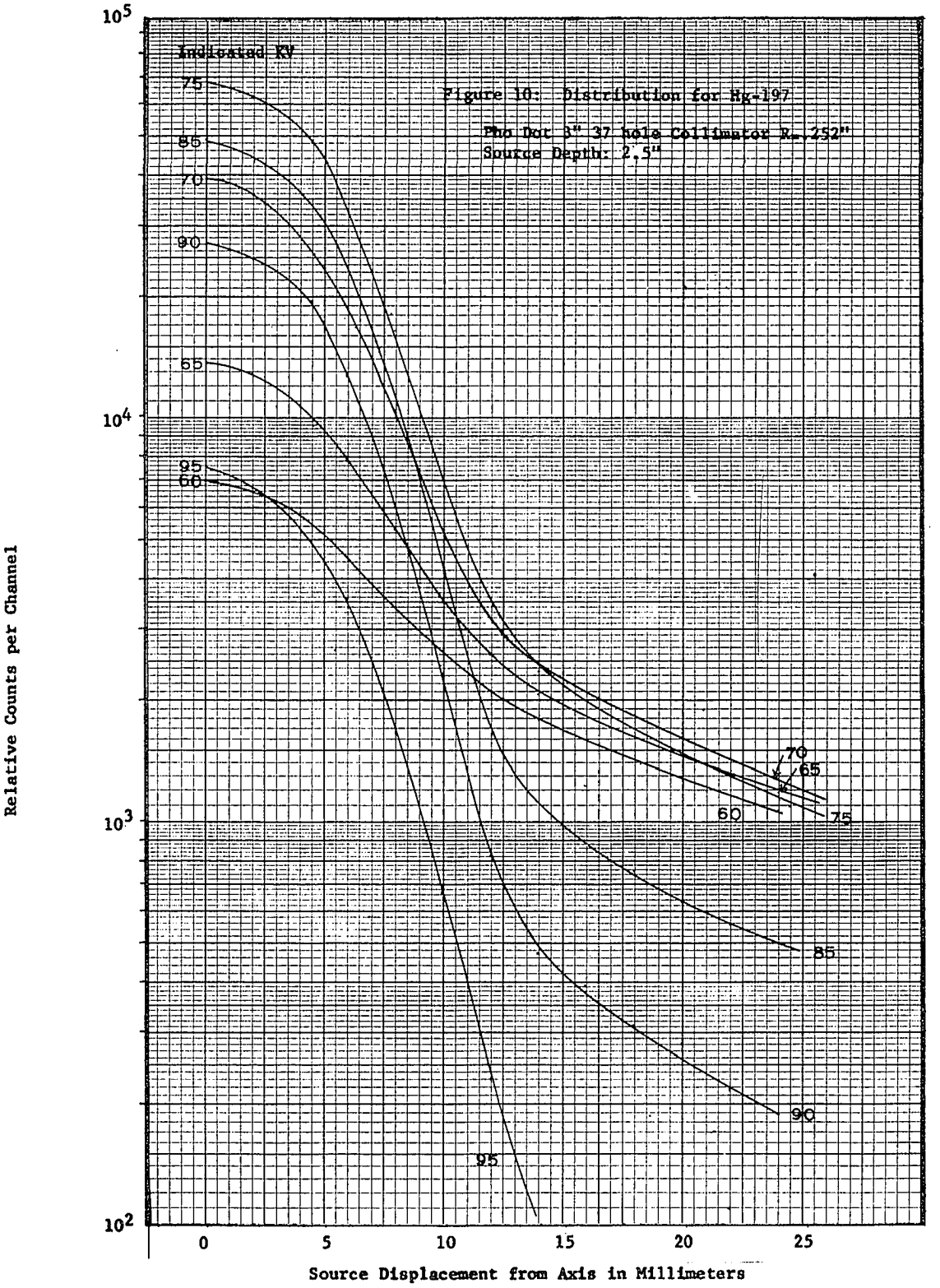
Figure 10: Distribution for Hg-197
Pho Dot 3" 37 hole Collimator R=.252"
Source Depth: 2.5"
Indicated KV
75
85
70
90
65
95
60
10^5
10^4
10^3
10^2
Relative Counts per Channel
0
5
10
15
20
25
Source Displacement from Axis in Millimeters

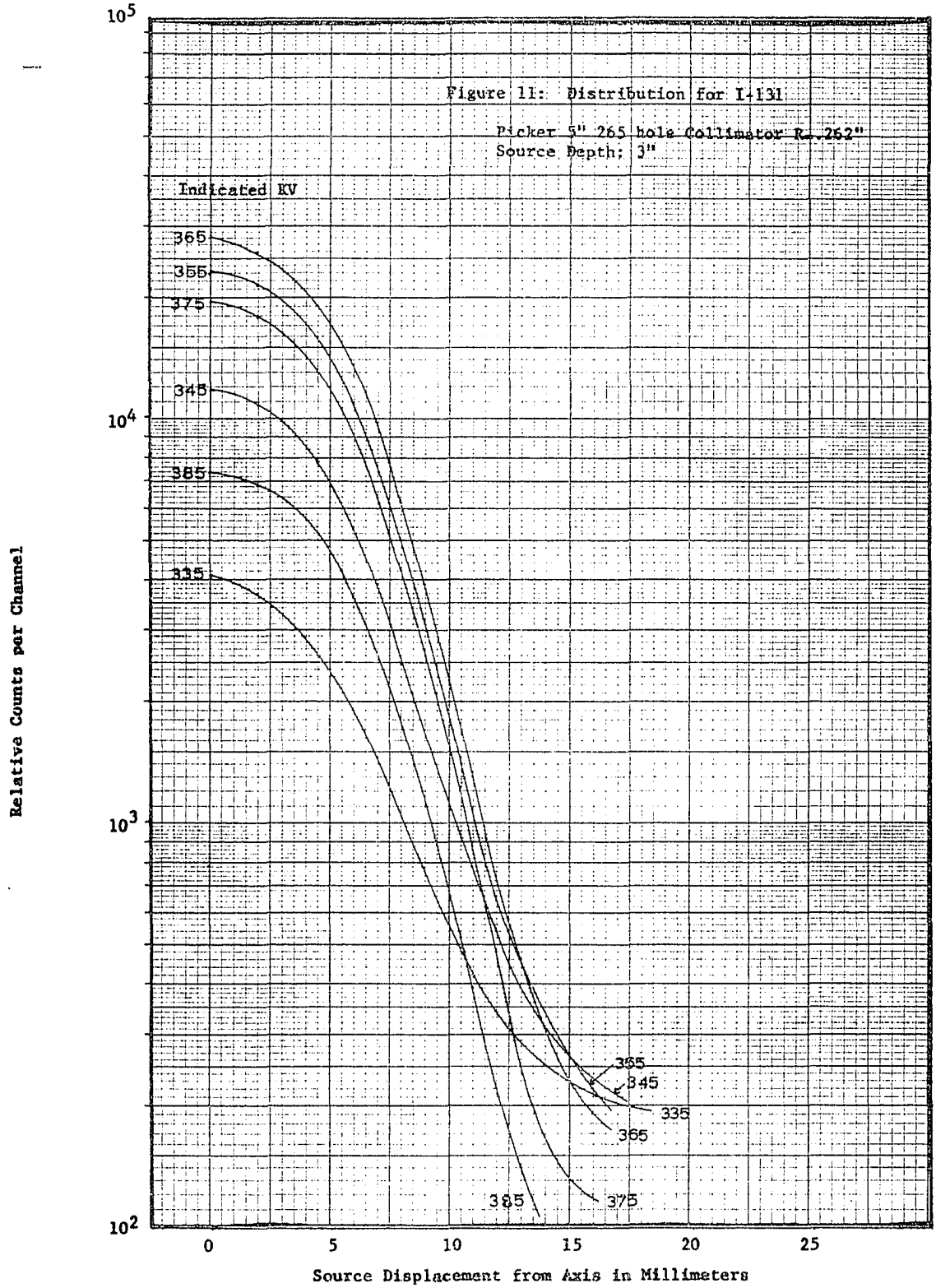
Figure 11: Distribution for I-131
Picker 5" 265 hole Collimator R=.262"
Source Depth; 3"
Indicated KV
365
355
375
345
385
335
10^5
10^4
10^3
10^2
Relative Counts per Channel
0
5
10
15
20
25
Source Displacement from Axis in Millimeters

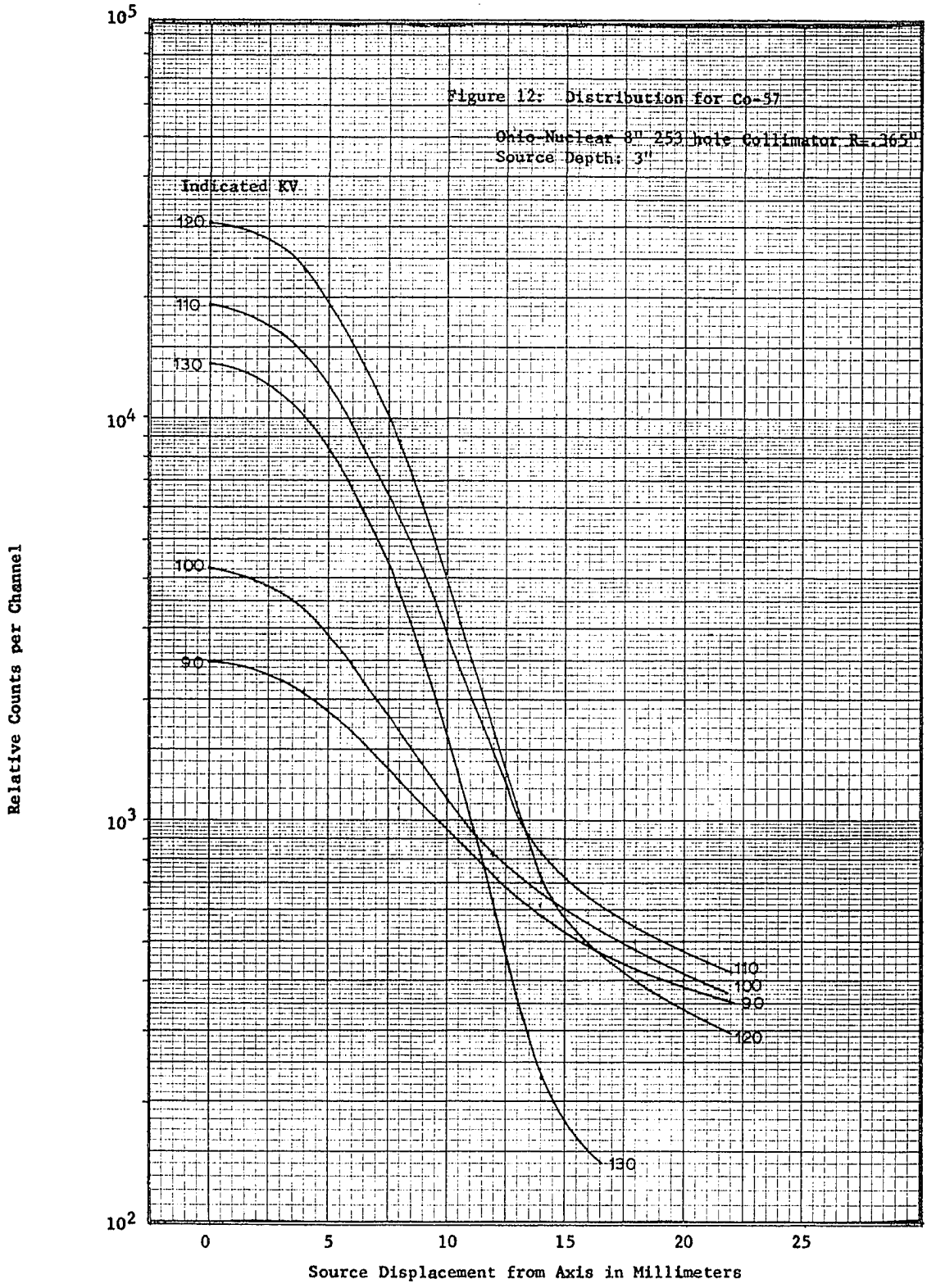
Figure 12: Distribution for Co-57
Ohio Nuclear 8" 253 hole Collimator R=.365"
Source Depth: 3"
Indicated KV
120
110
130
100
90
Relative Counts per Channel
10^5
10^4
10^3
10^2
110
100
90
120
130
0
5
10
15
20
25
Source Displacement from Axis in Millimeters

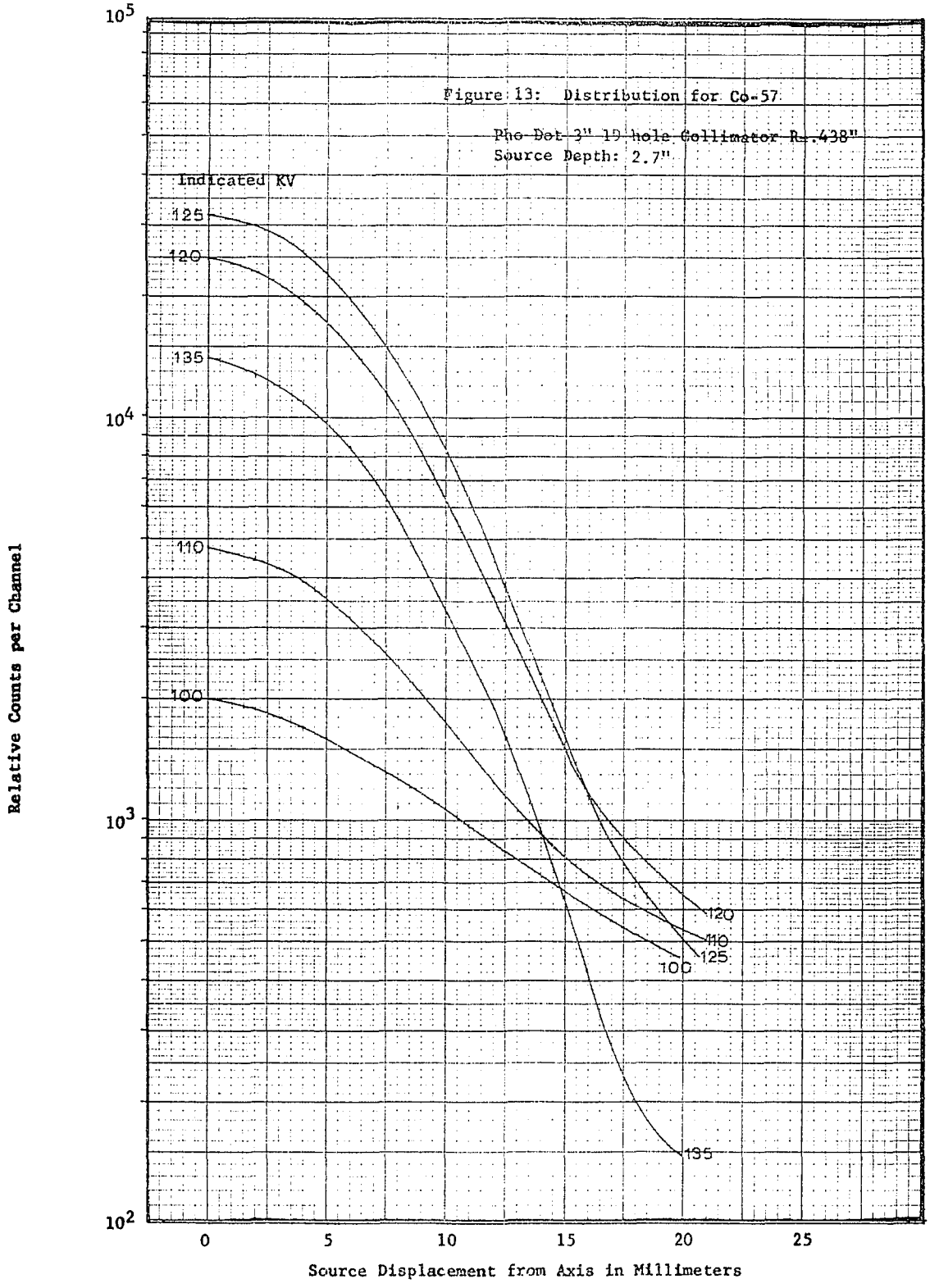
Figure 13: Distribution for Co-57
Pho-Dot 3" 19 hole Collimator R=.438"
Source Depth: 2.7"
Indicated KV
125
120
135
110
100
10^5
10^4
10^3
10^2
Relative Counts per Channel
0
5
10
15
20
25
Source Displacement from Axis in Millimeters

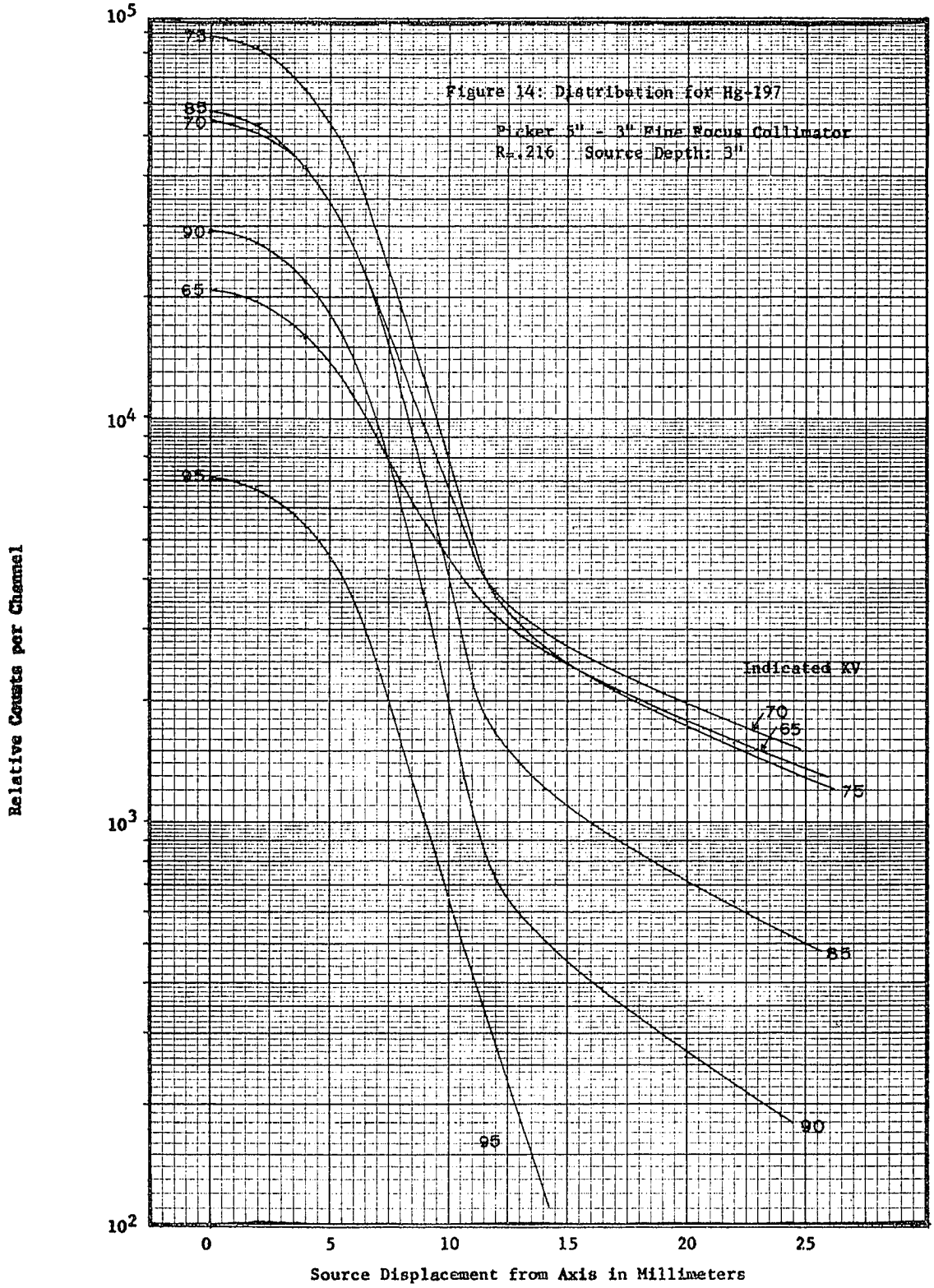
Figure 14: Distribution for Hg-197
Picker 5" - 3" Fine Focus Collimator
R=.216 Source Depth: 3"
Relative Counts per Channel
Source Displacement from Axis in Millimeters
Indicated KV
75
85
70
90
65
95
10^5
10^4
10^3
10^2
0
5
10
15
20
25

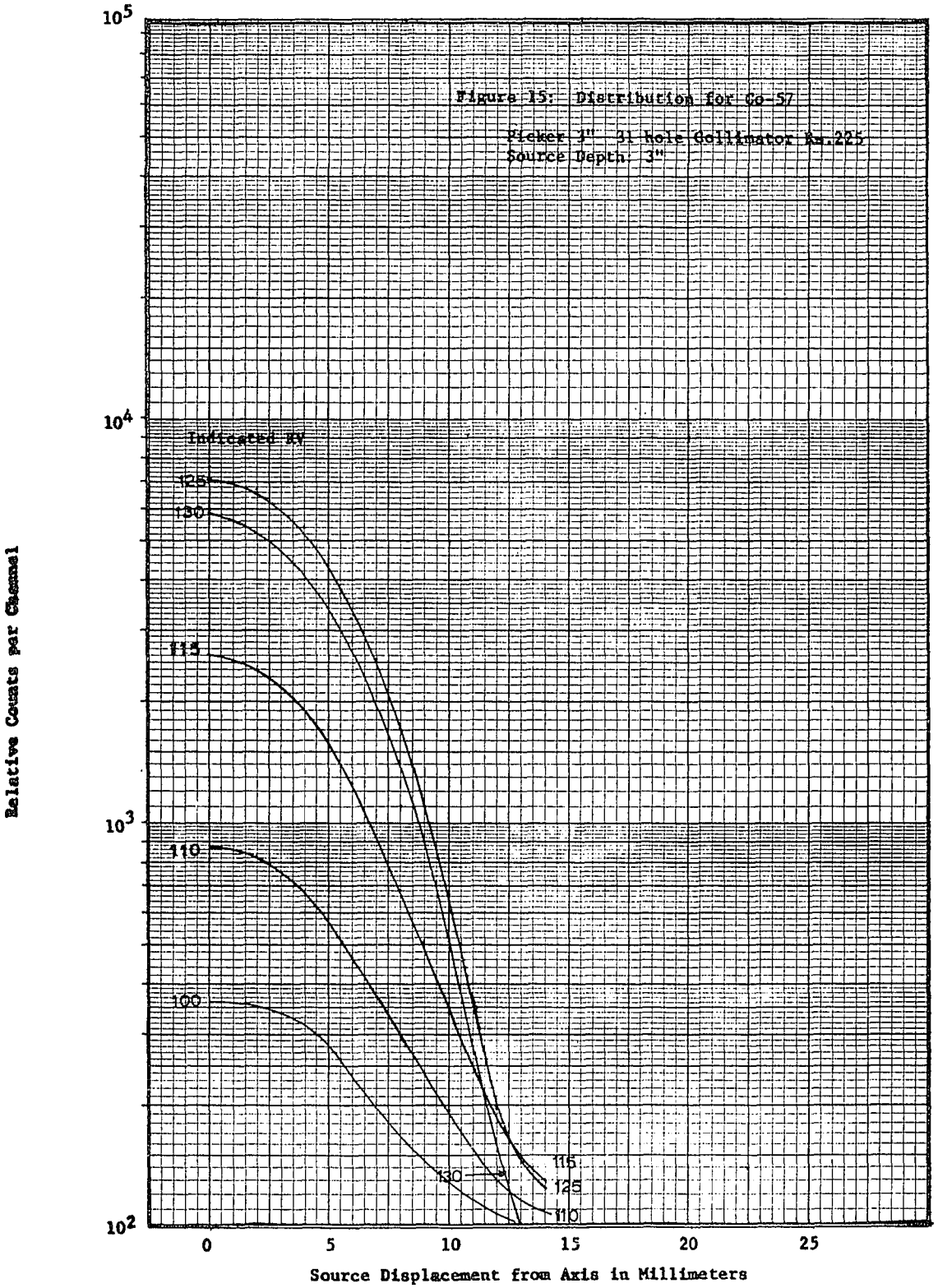
Figure 15: Distribution for Co-57
Picker 1" 31 Hole Collimator Rn.225
Source Depth: 3"
Relative Counts per Channel
10^5
10^4
10^3
10^2
Indicated KV
125
130
115
110
100
0
5
10
15
20
25
Source Displacement from Axis in Millimeters

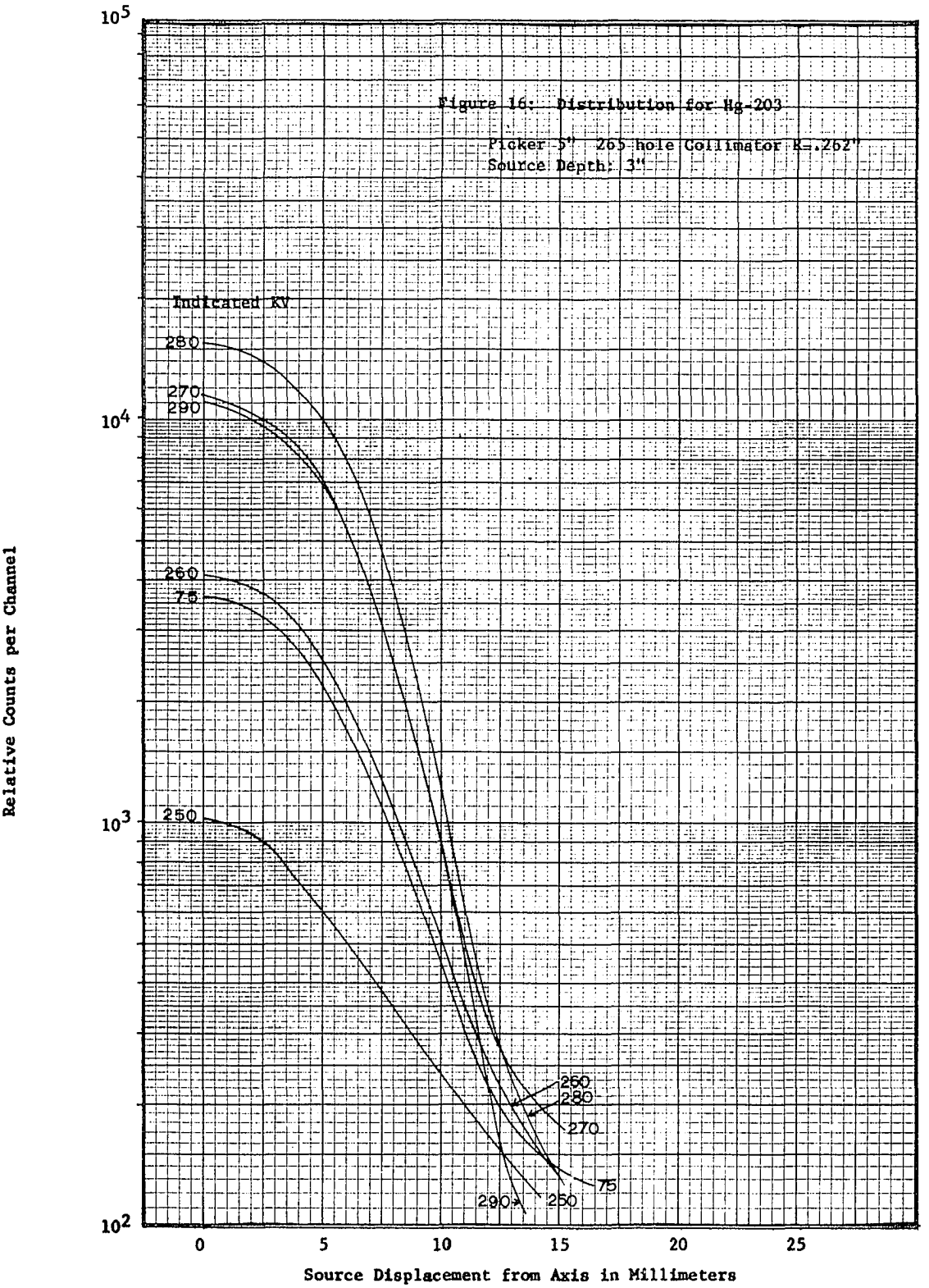
Figure 16: Distribution for Hg-203
Picker 5" 265 hole Collimator R=.262"
Source Depth: 3"
Indicated KV
280
270
290
260
75
250
290
250
280
270
75
250
10^5
10^4
10^3
10^2
0
5
10
15
20
25
Relative Counts per Channel
Source Displacement from Axis in Millimeters

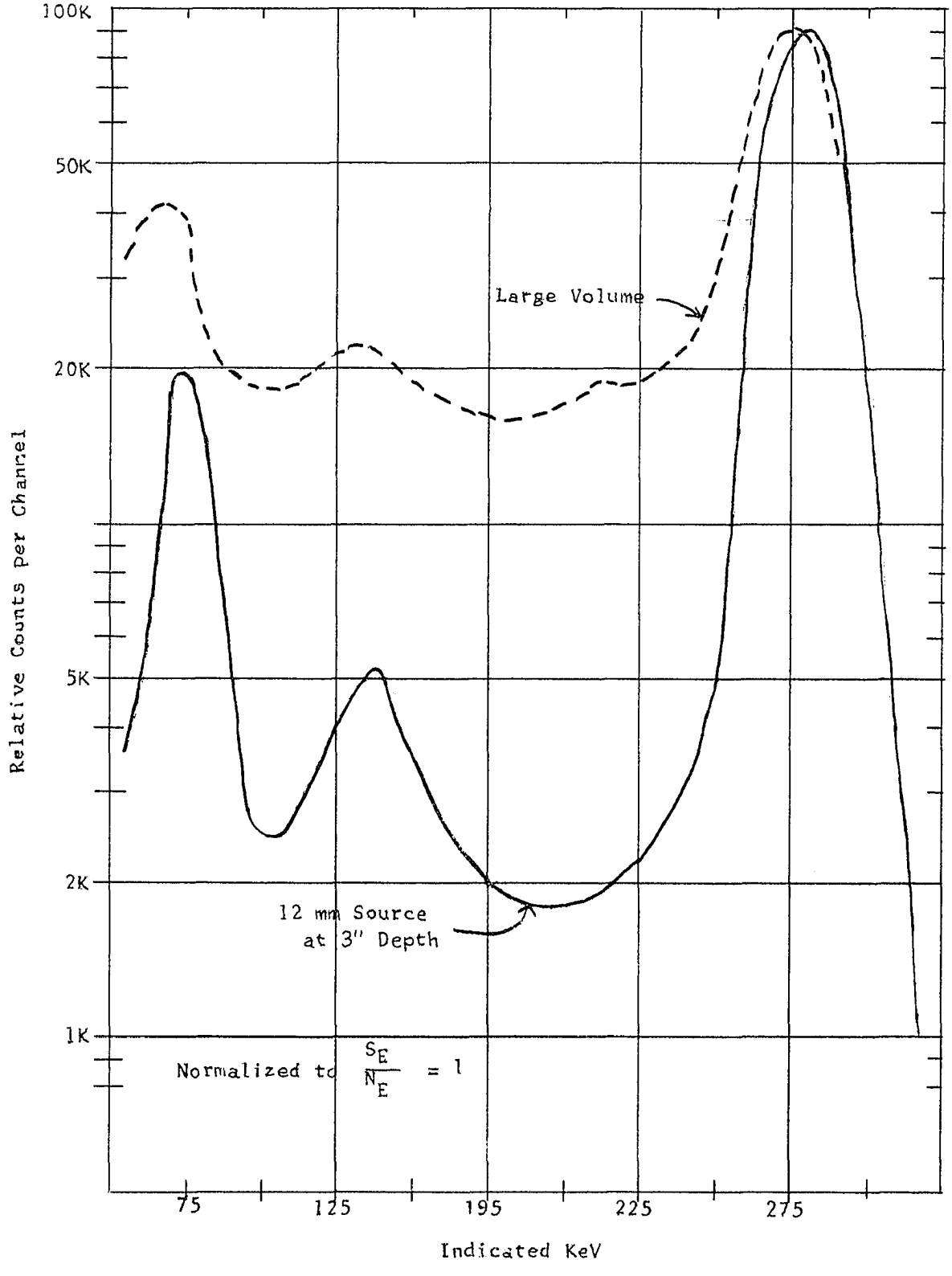

Figure 17: Large and Small Volume Scattering--Hg-203

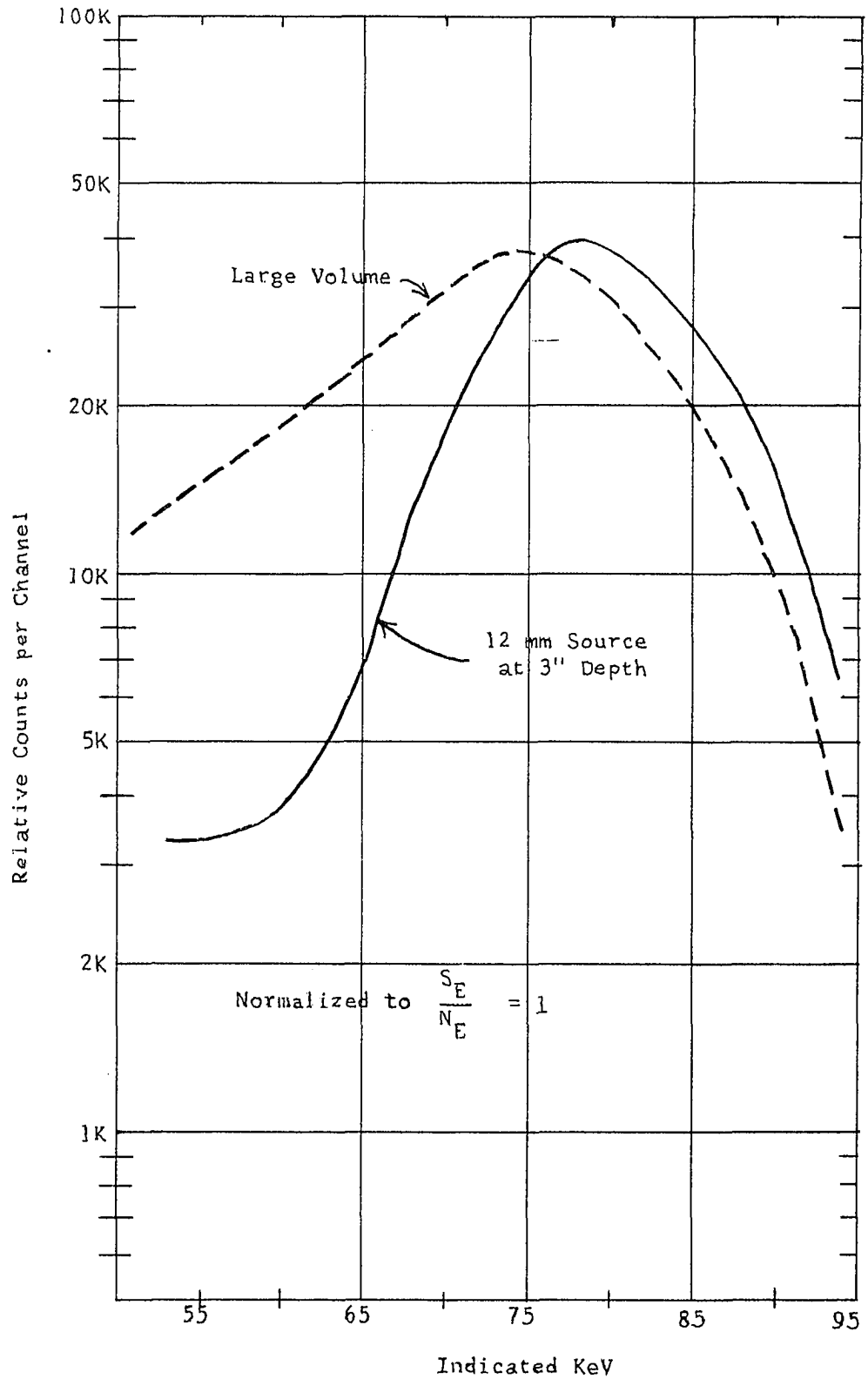

Figure 18: Large and Small Volume Scattering--Hg-197

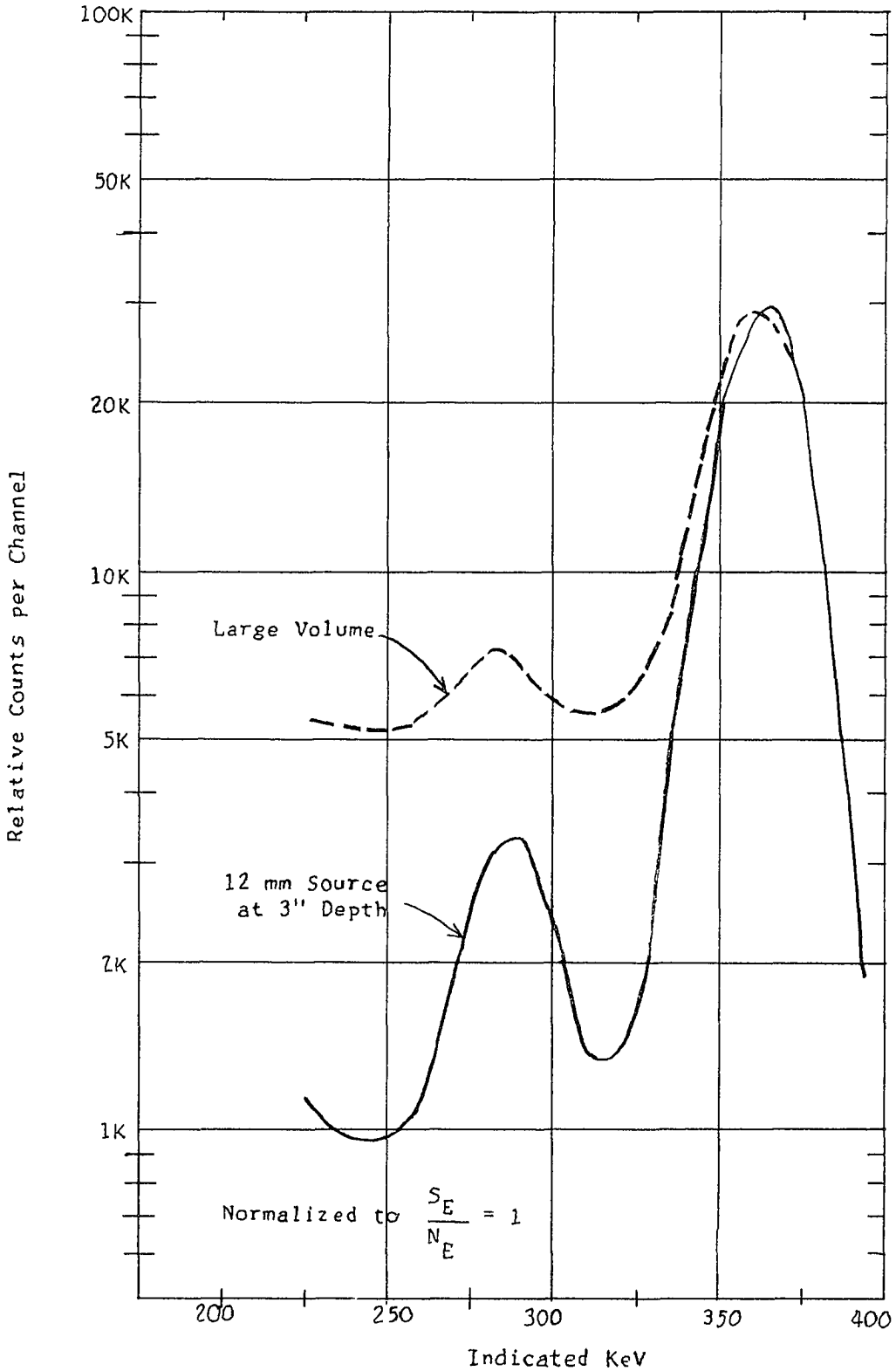

Figure 19: Large and Small Volume Scattering--I-131